NTNU – Trondheim
Norwegian University of
Science and Technology

Optimization of Well Spacing and CO2 Miscible Flooding Startup Time in an Ultradeep, High Pressure Oil Reservoir

Ahmad Hossein Zadeh

Petroleum Engineering
Submission date: July 2014
Supervisor: Jon Kleppe, IPT

Norwegian University of Science and Technology
Department of Petroleum Engineering and Applied Geophysics

Optimization of Well Spacing and CO_2 Miscible Flooding Startup Time in an Ultradeep, High Pressure Oil Reservoir

TPG4920 Petroleum Engineering, Master Thesis

Ahmad Hossein Zadeh

Norwegian University of Science and Technology

Faculty of Engineering Science and Technology

Department of Petroleum Engineering and Applied Geophysics

Supervisor: Professor Jon Kleppe

Trondheim, July 2014

Summary

Exploitation of ultradeep, high pressure oil reservoirs is always associated with numerous risks, challenges, and obstacles. One of the most pronounced constraints in development of such fields is the number of wells, which is imposed by massively high cost of drilling. Low number of wells may lead to high pressure isolation regions left after primary production (pressure depletion) of the reservoir. Ultradeep reservoirs with high pressure are more prone to such leftover high pressure isolation regions due to their low permeable characteristic. These high pressure isolation regions can, subsequently, deteriorate the efficiency of enhanced oil recovery (EOR) as the injected fluid cannot access the residual oil in these regions. Therefore, well placement and inter-well spacing optimizations is of greater importance in ultradeep, high pressure oil reservoirs to ensure higher ultimate oil recovery at lower costs. Furthermore, due to high cost of development of ultradeep, high pressure oil reservoirs, the EOR strategy and commencement time for the selected EOR strategy are very critical.

The objective of this thesis is to demonstrate how optimization of well placement, well spacing, and startup time for miscible CO_2 flooding can enhance the incremental and ultimate oil recoveries in an ultradeep, high pressure oil reservoir. To do this, a synthetic grid model was made to run different simulation scenarios on it. The model was initialized with rock and fluid properties within the range of those in the ultradeep, high pressure Wilcox formation in the Gulf of Mexico to ensure that it mimics an ultradeep, high pressure oil reservoir.

The obtained results showed that optimization of well placement, well spacing, and commencement time for any EOR strategy such as miscible CO_2 flooding is very critical in the course of making a Field Development Plan (FDP) for an ultradeep, high pressure oil reservoir.

The results, discussions, and conclusions were finally used by the author to shed light on potential further work on each of the aforementioned challenges in ultradeep, high pressure oil reservoirs such as Wilcox formation in the Gulf of Mexico.

Acknowledgements

I would like to express my greatest appreciation to my supervisor, Professor Jon Kleppe, for showing interest in the subject of my thesis and his subsequent supports and helps.

I would also like to thank Dr. Mohammad Ghasemi and Professor Curtis H. Whitson for providing me with valuable information and hints that helped me a lot in selection of the topic of my master thesis.

In addition, a thank you to all the administrative staff at the Department of Petroleum Engineering and Applied Geophysics in NTNU for their kind supports and helps.

Contents

List of Figures

List of Tables

Acronyms

BHP	Bottomhole Pressure
BML	Below the Mud Line
EOR	Enhanced Oil Recovery
EOS	Equation-of-State
FDP	Filed Development Plan
MME	Minimum Miscibility Enrichment
MMP	Minimum Miscibility Pressure
OOIP	Original Oil In Place
PVT	Pressure-Volume-Temperature
SSTVD	Sub-Sea True Vertical Depth
THP	Tubing Head Pressure

Nomenclature

γ_{API}	oil API gravity
γ_g	gas specific gravity
ΔR	incremental oil recovery
μ_g	gas viscosity
μ_o	oil viscosity
μ_{ob}	saturated oil viscosity
μ_{oD}	dead-oil viscosity
ρ_g	gas density
ρ_{pr}	pseudoreduced density
φ	porosity
ω	acentric factor
A	reservoir area
B_g	gas formation volume factor
B_{oi}	initial oil formation volume factor
c_i	volume shift
C_o	oil compressibility
CO_2	carbon dioxide
d	dimension
DX	length of grid blocks in X direction
DY	length of grid blocks in Y direction
h	reservoir thickness
J	well index
k_r	relative permeability
k_{rgro}	relative permeability of gas at S_w=S_{wc} and S_o= S_{org}
k_{rocw}	relative permeability of oil at S_w=S_{wc} and S_g= 0
k_{rwro}	relative permeability of water at S_w=1-S_{orw} and S_g=0
M	molecular weight

n	number of moles
n_g	gas exponent for analytical k_r
n_{og}	oil/gas exponent for analytical k_r
n_{ow}	oil/water exponent for analytical $kvolime_r$
n_w	water exponent for analytical k_r
NX	number of grid cells in X direction
NY	number of grid cells in Y direction
NZ	number of grid cells in Z direction
p	pressure
p_b	bubblepoint pressure
p_c	capillary pressure
p_{cr}	critical pressure
p_{pc}	pseudocritical pressure
p_{pr}	pseudoreduced pressure
p_r	reduced pressure
p_{sat}	saturation pressure
p_{sc}	standard conditions pressure
PV	pore volume
r_0	Peaceman's effective well radius
r_w	wellbore radius
R	universal gas constant
R_s	solution gas/oil ratio
S_{gc}	critical gas saturation
S_{gr}	trapped gas saturation
S_{org}	residual oil saturation to gas
S_{orw}	residual oil saturation to water
S_{wc}	connate water saturation
S_{wir}	irreducible/initial water saturation
t_D	EOR startup time

t_{EOR}	simulation run duration where economic limit is reached
T	temperature
T_{cr}	critical temperature
T_{pc}	pseudocritical temperature
T_{pr}	pseudoreduced temperature
T_r	reduced temperature
T_{sc}	standard conditions temperature
V	volume
Z	Z-factor
Z_c	critical Z-factor

Introduction

Outages in oil production due to political issues and declining conventional oil reservoirs in addition to struggles to catch up with global rising oil demand have given rise to approaching unconventional and difficult-to-develop oil resources. One type of difficult-to-develop oil resources is ultra deepwater oil reservoirs which are extremely costly and challenging to exploit. Some of the inherent characteristics of ultradeep oil reservoirs such as low permeability and high initial reservoir pressure, make drilling and extraction of oil from these reservoirs more challenging and expensive. A well-known example of such challenging reservoirs is Wilcox sandstone in the Gulf of Mexico with a permeability of typically less than 10 md, average oil viscosity of 5 cp, and initial reservoir pressure of about 20000 psi. Combining these characteristics with water depth of typically greater than 5000 ft and reservoir depth ranging from 25000 to 35000 ft below the mud line (BML) highlights the importance of optimization process in development of Wilcox sandstone to maximize the oil recovery at reduced costs.

Drilling wells in ultra deepwater, high pressure reservoirs has the highest contribution to field development costs. Therefore, one of the constraints in development of such reservoirs is the number of wells to drill. Low number of wells and improper well placement and inter-well spacing in addition to structural and stratigraphic controls that compartmentalize the reservoir can lead to localized pressure isolations at the end of primary production of high pressure reservoirs. These leftover high pressure regions not only may contain huge amounts of residual oil, but also can lead to high injection pressures required in the course of EOR processes. Therefore, new dedicated wells may be required to target the accumulations in the isolated regions and this imposes higher costs. This can be avoided by optimization of well placement and inter-well spacing for a given number of wells to drill in ultradeep, high pressure reservoirs in order to ensure maximized oil recovery at a minimum cost. Furthermore, to acquire the highest incremental production for an EOR strategy, the EOR commencement time should also be optimized.

The objective of this thesis is to demonstrate how optimization of well placement, inter-well spacing, and EOR startup time lead to maximized ultimate and incremental oil productions in an ultradeep, high pressure oil reservoir. The EOR process in this study is miscible CO_2

injection and due to high-pressure characteristic of the reservoir, no secondary oil production is considered for the reservoir model under study.

According to Muskat (1949), the well spacing problem can be approached from two different perspectives: the physical ultimate recovery and economic ultimate recovery. The optimization in this study was conducted based on the physical ultimate recovery obtained from reservoir simulation. Therefore, the optimal well spacing defined in this report is only based on the volume of oil produced and does not consider the maximum economic return from the development of the reservoir.

Due to lack of real data, a synthetic cubic model was made and it was initialized with the reservoir properties within the range of those of the ultradeep, high pressure Wilcox formation in the Gulf of Mexico to ensure that the model mimics an ultradeep, high pressure oil reservoir. The black oil table required for black oil simulations was made using the available correlations and limited available data on Wilcox in literature. For the compositional model, we had to make up a fluid composition and EOS which generated the black oil table made based on the limited data available in open literature.

Inter-well spacing and EOR startup time optimization was done for four different well patterns on the reservoir model to achieve the objective of the study. In order to reduce the simulation cost and numerical dispersion imposed by the constraint on the number of grid cells (6000 grid cells for SENSOR) the optimization was performed for a given well pattern on a section of the reservoir using the concept of symmetry.

The report is outlined as explained in the following paragraphs.

Chapter 1 is a precise literature review to the extent that might be required by the reader to understand the contents of the next chapters.

Chapter 2 explains how the black oil and compositional models were made using the correlations given in Chapter 1. The grid model is also discussed in this chapter.

Chapter 3 gives an explanation on the optimization strategy used in the study.

Chapter 4 covers the optimization process and the corresponding results.

In **Chapter 5**, integrates the conclusions that can be made based on the results obtained in the previous chapter.

In **Chapter 6**, outlines the recommendations made based on the conclusions drawn in the previous chapter. The goal of this chapter is to draw the reader's attention to the potential areas of research similar to this thesis subject.

Chapter 1: Literature Review

This chapter covers the background information from literature review which will be used in the discussions in the next chapters.

1.1 Oil and Gas Properties and Correlations

This section gives definitions and correlations for the required PVT properties of oil and natural gases to make the black oil PVT table for the model under study.

1.1.1 Critical and Reduced Properties

Reduced temperature (T_r) and reduced pressure (p_r) are dimensionless properties of a pure component and are defined as

$$T_r = \frac{T}{T_{cr}} \tag{1.1}$$

$$p_r = \frac{p}{p_{cr}}. \tag{1.2}$$

Absolute units must be used whilst calculating reduced temperature and pressure. p_{cr} and T_{cr} are the true critical properties of a pure component. In most petroleum engineering applications, p_r ranges from 0.02 to 30 for gases and 0.03 to 40 for oils and T_r ranges from <1 to 0.25 for gases and from 0.4 to 1.1 for oils (Whitson and Brule´ 2000).

1.1.2 Gas Pseudocritical and Pseudoreduced Properties

Average hydrocarbon gas mixture critical properties, known as pseudocritical properties (p_{pc} and T_{pc}), can be obtained from mixture specific gravity.

Sutton (1985) presented the following correlations for estimation of p_{pc} and T_{pc} of hydrocarbon gas mixtures, knowing the hydrocarbon gas mixture specific gravity (γ_g).

$$T_{pc} = 169.2 + 349.5\gamma_g - 74.0\gamma_g^2 \tag{1.3}$$

$$p_{pc} = 756.8 - 131.0\gamma_g - 3.6\gamma_g^2 \tag{1.4}$$

Standing (1981) suggested the following two correlations for dry hydrocarbon gases (γ_g<0.75).

$$T_{pc} = 168.0 + 325.0\gamma_g - 12.5\gamma_g^2 \tag{1.5}$$

$$p_{pc} = 667.0 - 15.0\gamma_g - 37.5\gamma_g^2 \tag{1.6}$$

The Standing correlations are used in the industry extensively.

Pseudocritical properties of hydrocarbon gas mixtures are used to calculate pseudoreduced temperature and pseudoreduced pressure for the gas mixture using **Eqs. 1.7 and 1.8**.

$$T_{pr} = \frac{T}{T_{pc}}$$

(1.7)

$$p_{pr} = \frac{p}{p_{pc}} \tag{1.8}$$

1.1.3 Gas Deviation Factor

According to the ideal-gas law,

$$pV = nRT, \tag{1.9}$$

where R is the universal gas constant.

At moderate to high pressure or at low temperatures, volume of constituting molecules of a gas mixture and the corresponding intermolecular forces affect the volumetric behavior of the gas and the ideal-gas law does not hold anymore. The deviation from ideal-gas law can be expressed by gas deviation factor, also known as *Z*-factor. By definition,

$$Z = \frac{volume\ \ of\ \ one\ \ mole\ \ of\ \ real\ \ gas\ \ at\ \ p\ \ and\ \ T}{volume\ \ of\ \ one\ \ mole\ \ of\ \ ideal\ \ gas\ \ at\ \ p\ \ and\ \ T}. \tag{1.10}$$

According to the definition of *Z*-factor, this parameter is unitless.

Having pseudoreduced pressure and temperature of a given hydrocarbon gas mixture, one can use Standing-Katz *Z*-factor chart **(Fig. 1)** to estimate the *Z*-factor for that mixture.

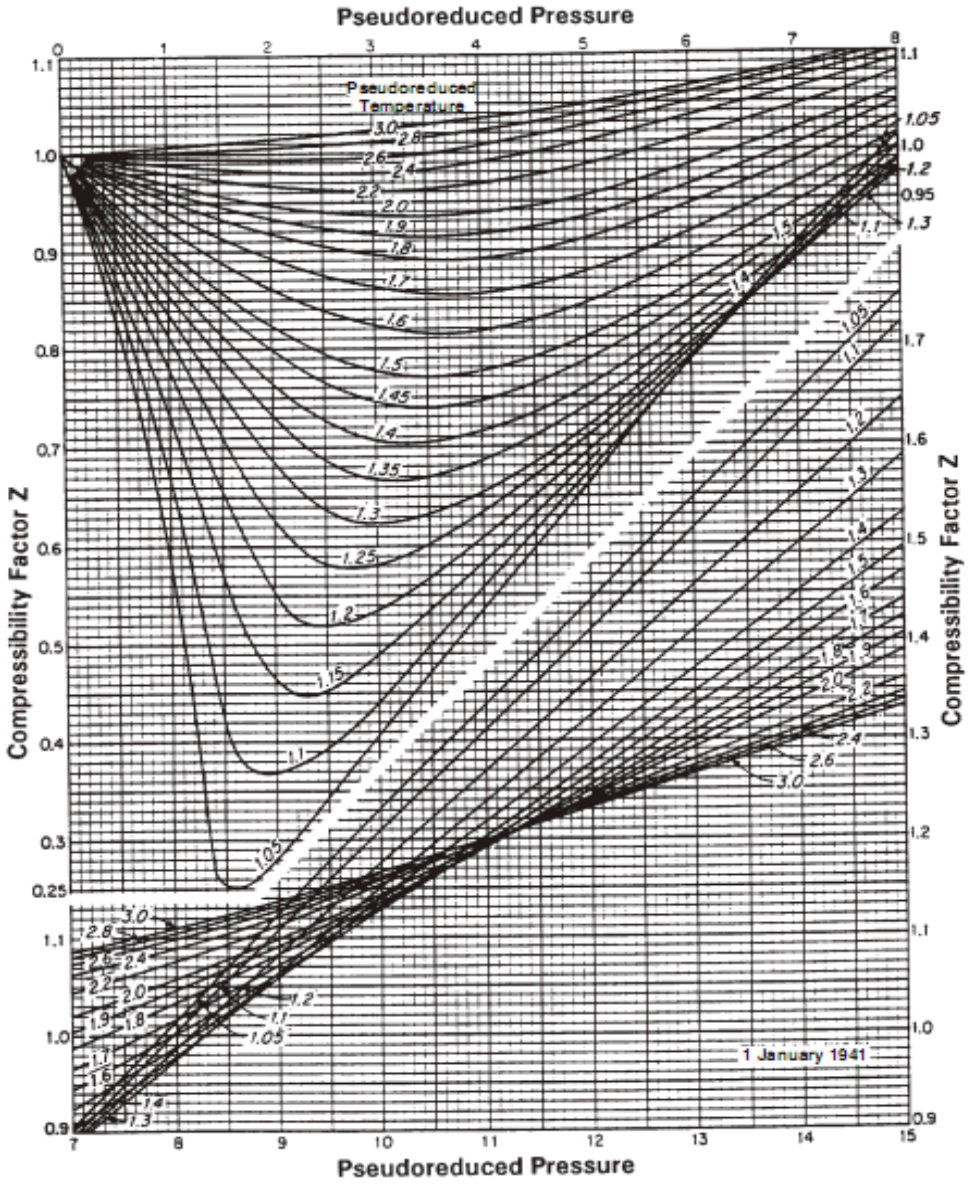

Figure 1 - Standing-Katz Z-factor Chart (Whitson and Brule´ 2000)

Sutton (1985) claimed that his suggested correlations **(Eqs. 1.3 and 1.4)** are the most reliable correlations for estimating *Z*-factor with the Standing-Katz *Z*-factor chart.

Dranchuk and Abou-Kassem (1975) fitted one of the most accurate equations-of-state to the Standing-Katz *Z*-factor chart, which is more convenient for estimating the *Z*-factor for a gas mixture. Their equation is expressed as follows:

$$Z = 1 + (A_1 + \frac{A_2}{T_{pr}} + \frac{A_3}{T_{pr}^3} + \frac{A_4}{T_{pr}^4} + \frac{A_5}{T_{pr}^5})\rho_{pr} + (A_6 + \frac{A_7}{T_{pr}} + \frac{A_8}{T_{pr}^2})\rho_{pr} - A_9(\frac{A_7}{T_{pr}} + \frac{A_8}{T_{pr}^2})\rho_{pr}^5$$

$$+A_{10}(1 + A_{11}\rho_{pr}^2)(\frac{\rho_{pr}^2}{T_{pr}^3})\exp(-A_{11}\rho_{pr}^2), \quad (1.11)$$

where

$$\rho_{pr} = \frac{0.27 p_{pr}}{Z T_{pr}} \quad (1.11a)$$

and where the constants A_1 to A_{11} are as follows:

A_1 = 0.3265,

A_2 = -1.0700,

A_3 = -0.5339,

A_4 = 0.0157,

A_5 = -0.0517,

A_6 = 0.5475,

A_7 = -0.7361,

A_8 = 0.1844,

A_9= 0.1056,

A_{10}= 0.6134,

and A_{11}= 0.7210.

Dranchuk and Abou-Kassem equation can be used for a broad range of pressures and temperatures and is valid for $0.2 \le p_{pr} \le 30$ and $1.0 \le T_{pr} \le 3.0$ and for $p_{pr} \le 1$ with $0.7 \le T_{pr} \le 1.0$.

1.1.4 Gas Density

One can derive all volumetric properties of gases from the real gas law. Gas density, ρ_g, is given by

$$\rho_g = \frac{pM_g}{ZRT}. \quad (1.12)$$

Alternatively, in terms of gas specific gravity,

$$\rho_g = 28.97\frac{p\gamma_g}{ZRT}. \tag{1.13}$$

in which p is in psia, R is in (psia.ft^3)/(^{o}R.lb-mol), T is in ^{o}R, and ρ_g is in lb$_m$/ft^3.

1.1.5 Gas Formation Volume Factor

By definition, gas formation volume factor, B_g, is the ratio of gas volume at specific temperature and pressure (e.g. reservoir temperature and pressure) to the ideal-gas volume at standard conditions. Therefore, B_g is given by

$$B_g = \frac{ZTp_{sc}}{pT_{sc}}. \tag{1.14}$$

1.1.6 Gas Viscosity

Typical reservoir gas viscosities range from 0.01 to 0.03 cp at standard and reservoir conditions, reaching up to o.1 cp for near critical gas condensate (Whitson and Brule´ 2000).

Lee-Gonzalez (1966) suggested a gas viscosity correlation **(Eq. 1.15)** which is nowadays the most commonly used correlation in PVT laboratories.

$$\mu_g = A_1 x 10^{-4} \exp(A_2 \rho_g^{A_3}) \tag{1.15}$$

where

$$A_1 = \frac{(9.379 + 0.01607M_g)T^{1.5}}{209.2 + 19.26M_g + T}, \tag{1.15a}$$

$$A_2 = 3.448 + (986.4/T) + 0.01009M_g, \tag{1.15b}$$

and

$$A_1 = 2.447 - 0.2224A_2. \tag{1.15c}$$

In Lee-Gonzalez gas viscosity correlation, μ_g is in cp, ρ_g is in g/cm^3, and T is in ^{o}R. McCain (1991) showed that the accuracy of Lee-Gonzalez correlation is 2 to 4% for γ_g <1.

1.1.7 Solution Gas/Oil Ratio

Solution gas/oil ratio, R_s, is the volume of gas at standard conditions librated from a single-phase oil at elevated pressure and temperature (e.g. reservoir pressure and temperature) divided by the resulting stock-tank oil volume, with units scf/STB (Whitson and Brule´ 2000).

1.1.8 Bubblepoint Pressure

Petrosky and Farshad (1993) presented a correlation for estimating bubblepoint pressure for the Gulf of Mexico crude oils. They claimed that their correlation provided improved results for the Gulf of Mexico oils compared to other correlations developed by other researchers for California oils, North Sea oils, etc. Their correlation gives

$$p_b = 112.727\left(\frac{R_s^{0.5774}}{\gamma_g^{0.8439}} 10^x - 12.34\right), \tag{1016}$$

where

$$x = 0.00004561T^{13911} - 0.0007916\gamma_{API}^{1.541}. \tag{1.16a}$$

In Petrosky and Farshad correlation, $R_s$is in scf/STB, T is in ^{o}F, and p_b is in psia.

1.1.9 Oil Viscosity

Based on the curve fitting of the undersaturated oil viscosity versus pressure data presented by Beal (1946), Standing (1981) suggested the following correlation for estimation of undersaturated oil viscosities.

$$\frac{\mu_o - \mu_{ob}}{0.001(p - p_b)} = 0.024\mu_{ob}^{1.6} + 0.038\mu_{ob}^{0.56} \tag{1.17}$$

Chew and Connally (1959) tried to correlate saturated oil viscosity with dead-oil viscosity. They proposed the following correlation.

$$\mu_{ob} = A_1\mu_{oD}^{A_2} \tag{1.18}$$

Different researchers tried to present mathematical relations for A_1 and A_2 in Chew and Connally correlation. For example, Standing (1981) suggested the following relations in terms of *Rs* for A_1 and A_2.

$$A_1 = 10^{-(0.00074R_s + 0.00000022R_s^2)} \tag{18a}$$

$$A_2 = \frac{0.68}{10^{0.0000862R_s}} + \frac{0.25}{10^{0.0011R_s}} + \frac{0.062}{10^{0.00374R_s}} \tag{18b}$$

1.1.10 Oil Compressibility

Petrosky and Farshad (1993) proposed the following correlation for estimation of oil compressibility of undersaturated oils in the Gulf of Mexico.

$$c_o = 1.705x10^{-7} R_{sb}^{0.69357} \gamma_g^{0.1885} \gamma_{API}^{0.3272} T^{0.6729} p^{-0.5906} \tag{1.19}$$

where $2.464\text{x}10^{-5} < c_o < 3.507\text{x}10^{-5}$.

Vasquez and Beggs (1980) also suggested a more general correlation **(Eq. 1.20)** for prediction of undersaturated oil compressibility.

$$c_o = \frac{-1433 + 5R_s + 17.2T - 1180\gamma_g + 12.61\gamma_o}{10^5 p} \tag{1.20}$$

1.1.11 Oil Formation Volume Factor

Oil formation volume factor ranges from 1 bbl/STB for oils with little solution gas to about 2.5 bbl/STB for volatile oils (Whitson and Brule´ 2000).

Petrosky and Farshad (1993) correlation for estimation of bubblepoint oil formation volume factor for Gulf of Mexico crude oils is

$$B_{ob} = 0.9759 + 0.00012A^{1.2} \tag{1.21}$$

where

$$A = R_s(\gamma_g / \gamma_o)^{0.5} + 1.25T\,. \tag{1.21a}$$

One can use oil compressibility and bubblepoint oil formation volume factor to calculate the variations in oil formation volume factor using **Eq. 1.22**.

$$B_o = B_{ob} \exp[c_o(p_b - p)] \tag{1.22}$$

1.2 Miscibility

Miscibility is different from solubility. Two fluids are said to be miscible when they combine in any proportion to form one phase. For example water and methanol are two miscible fluids. But if a fluid gets dissolved in another fluid up to a certain proportion, it is said to be soluble in the other fluid. Solubility is a function of the nature of fluids, temperature, and pressure. An intermediate phenomenon is known as dynamic miscibility where miscibility is attained gradually, through multi-contact, and involves extraction or vaporization of light ends (Khatib et al. 1981).

Miscibility can be achieved either by first-contact (absolute) miscibility process or by a multiple-contact (thermodynamic) miscibility process. First-contact miscibility is a condition in which the injected gas (solvent) and oil are miscible (i.e. they form a single phase when mixed in any proportion when first brought into contact at a given pressure and temperature). Condition of first-contact miscibility for reservoir gasflooding depends on the composition of the injected gas, composition of oil, temperature, and the injection pressure. By contrast, fluids that develop miscibility after exchanging components have multiple-contact miscibility (Oilfield Glossary, First-Contact Miscibility 2013). Multiple-contact (dynamic) miscibility is a dynamic fluid-mixing process in which the injected gas exchanges components with in situ oil until the phases achieve a state of miscibility within the mixing zone of the flood front. In a vaporizing drive, light and intermediate components from the oil phase enter the gas phase. By contrast, in a condensing drive, intermediate components from the gas phase enter the oil phase. The process may be a combination of vaporizing and condensing drives (Oilfield Glossary, Multiple-Contact Miscibility 2013).

1.2.1 Minimum Miscibility Pressure (MMP)

Figure 6 shows a series of hypothetical slimtube experiments. In these experiments, the solvent displaces oil from the fully oil-saturated slimtube at several pressures. Oil recovery is shown after 1.2 pore volume (PV) of injection for each pressure. Oil recovery increases with pressure up to approximately 95 to 98% and then increases very little thereafter. The pressure at which the break in the recovery curve occurs is called the minimum miscibility pressure (MMP). If the displacements had been conducted at constant pressure and with increasing enrichment by components such as ethane, propane, and butane, the break would have been at the minimum miscibility enrichment (MME). Above the MMP or MME, the displacement is said to be multiple-contact or dynamically miscible. The increasing recovery with pressure or solvent enrichment results from in-situ mass transfer of components between solvent and resident oil. Each pressure increase produces an equilibrium mixture that becomes compositionally similar at the MMP or MME (Petrowiki, Miscible Flooding 2013).

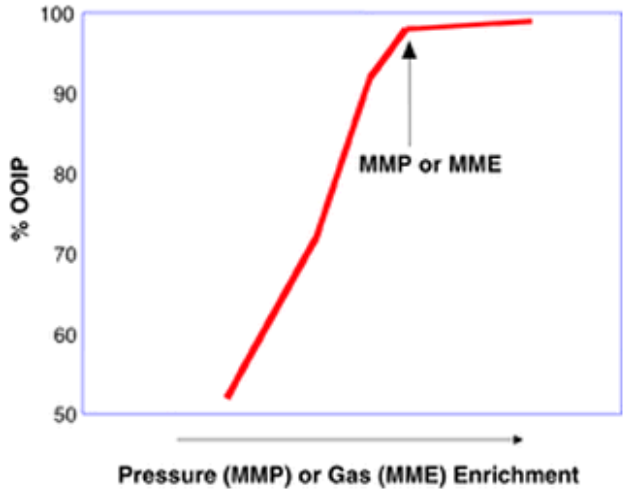

Figure 2 - Slimtube displacements used to determine MMP or MME (Petrowiki, Miscible Flooding 2013)

It should be noted that a slimtube test cannot fully represent the performance in reservoir rock because it does not account for the effects of factors such as gravity segregation and reservoir heterogeneity on volumetric sweep (Petrowiki, Miscible Flooding 2013).

CO_2 flooding is applicable with medium-gravity oils. At temperatures less than approximately 125°F, MMP is estimated to be as low as 1200 psia. MMP increases with temperature. (Petrowiki, Designing a Miscible Flood 2013).

1.2.2 Effect of Numerical Dispersion on Miscible Gas Injection Simulation

Miscible gas injection is one of the most promising EOR techniques which was invented many years ago and since 1950s it has been implemented in many places around the world.

From a reservoir simulation standpoint, one of the main factors affecting recovery calculations by simulation of a miscible solvent injection is grid refinement. Numerical dispersion due to large grid block size, greatly affects oil/gas miscibility in reservoir simulation of 1D displacement. This, in consequence, results in reduction of local displacement efficiency. Therefore, refinement of grid cells can diminish the effect of numerical dispersion in reservoir simulations (Johns et al. 1992; Haajizadeh et al. 1999; Solano et al. 2001). However, different studies (Stalkup 1990; Lim et al. 1997; Haajizadeh et al. 2000) on the effect of numerical dispersion on 2D displacement efficiency for miscible gas flooding drew different conclusions about if very small grid blocks can diminish the error introduced by numerical dispersion in reservoir simulation of 2D displacement. It seems that the sensitivity of recovery to grid refinement for miscible flooding is a function of injection conditions and reservoir descriptions.

1.3 SENSOR Reservoir Simulator

SENSOR is a generalized 3D numerical reservoir simulation model for simulating compositional and black oil problems.

1.3.1 SENSOR Data File Structure

SENSOR data file consists of 3 main sections:

- Initial Data: The data file starts with TITLE/alphanumeric lines/ENDTITLE, followed by GRID N_X N_y N_z, and remaining Initial Data. The Initial Data ends with the keyword ENDINIT.
- Modification Data: The Modification Data, if present, start with the keyword MODIFY, following ENDINIT.
- Recurrent Data: Recurrent Data normally start with the keyword WELL, and end with the keyword END, which is the last keyword in the data file.

All the keywords in SENSOR data file are upper case. Apart from the PVT data, there are almost no differences in the data input for black oil and compositional problems (INITIAL data formats and specifications for injected gas composition differ). Comments may be included on any keyword or data line following an !. A comment line is one where the first character on the line is a ‘‘C’’ or ‘‘c’’, followed by one or more blanks.

The general layout of SENSOR data file is shown in Appendix 1.

1.3.2 Analytical Relative Permeability and Capillary Pressure Curves in SENSOR

In research problems or in case of occurrence of large scatter and uncertainty in relative permeability data, analytical relative permeability (k_r) and capillary pressure (p_c) data are often used. Using analytical expressions makes it easy to change k_r data for the purpose of sensitivity runs and history matching.

Endpoint saturations and curvature are the most important properties of k_r curves. KRANALYTICAL keyword in SENSOR is used to represent these properties using the minimum number of variables.

To use the analytical k_r data, the following variables should be entered:

S_{wc}: connate water saturation

S_{orw}: residual oil saturation to water

S_{org}: residual oil saturation to gas

S_{gc}: critical gas saturation

S_{gr}: trapped gas saturation, optional, default=S_{gc}

k_{rwro}: relative permeability of water at S_w=1-S_{orw} and S_g=0

k_{rgro}: relative permeability of gas at S_w=S_{wc} and S_o= S_{org}

k_{rocw}: relative permeability of oil at S_w=S_{wc} and S_g= 0

n_w, n_{ow}, n_g, and n_{og}: exponents for analytical k_r

The relative permeabilities are calculated by SENSOR as

$$k_{rw} = k_{rwro}[(S_w - S_{wc}) / (1 - S_{orw} - S_{wc})]^{n_w} \quad (1.23)$$

$$k_{row} = k_{rocw}[(1 - S_{orw} - S_w) / (1 - S_{orw} - S_{wc})]^{n_{ow}} \quad (1.24)$$

$$k_{rog} = k_{rocw}[(1 - S_{org} - S_{wc} - S_g) / (1 - S_{org} - S_{wc})]^{n_{og}} \quad (1.25)$$

$$k_{rg} = k_{rgro}[(S_g - S_{gc}) / (1 - S_{org} - S_{wc} - S_{gc})]^{n_g} \quad (1.26)$$

Analytical p_c are calculated by SENSOR as

$$p_{cwo} = A_1 + A_2(1 - S_{wn})^{A_3} \quad (1.27)$$

$$p_{cwoi} = B_1 + B_2(1 - S_{wn})^{B_3} - B_4 S_{wn}^{B_5} \quad (1.28)$$

$$p_{cgo} = C_1 + C_2 S_{gn}^{C_3} \quad (1.29)$$

where

p_{cwo}: drainage water/oil p_c

p_{cwoi}: imbibition water/oil p_c

p_{cgo}: drainage gas/oil p_c

$$S_{wn} = (S_w - S_{wc}) / (1 - S_{wc}) \quad (1.30)$$

$$S_{gn} = S_g / (1 - S_{wc}) \quad (1.31)$$

A_1 to A_3, B_1 to B_5, and C_1 to C_3 are variables entered for PCWO, PCWOI, and PCGO keywords.

1.4 Well Productivity Index Calculations

Well index (J) can be calculated using the formulae **(Eq. 1.32)** presented by Peaceman (1983). Assume that the wellbore penetrates the center of a grid block in any direction, X, Y, or Z. The wellbore direction is labeled direction 3 and the directions in the plane perpendicular to the wellbore are labeled directions 1 and 2. Considering this convention, block permeability and dimensions in directions 1, 2, and 3 are k_1, k_2, and k_3 and d_1, d_2, and d_3, respectively. Peaceman's formula for an anisotropic case ($k_1 \neq k_2$) is

$$J = 0.00708 k d_3 / (\ln(r_0 / r_w) + s) \tag{1.32}$$

where

$k = \sqrt{k_1 k_2}$, k and d are in units of md and ft, and

$$r_0 = 0.28\ [(k_2 / k_1)^{0.5} d_1^2 + (k_1 / k_2)^{0.5} d_2^2]^{0.5} / [(k_2 / k_1)^{0.25} + (k_1 / k_2)^{0.25}] \tag{1.33}$$

For an isotropic case ($k_1 = k_2$), **Eq. 1.33** is reduced to

$$r_0 = 0.14\ (h_1^2 + h_2^2)^{0.5} \tag{1.34}$$

Chapter 2: Model Preparations

This chapter presents the methodology used for making the two fundamental components of the simulation model: PVT data and grid model. Furthermore, other components of the model such as well data (productivity index, perforations, well constraints, etc.) are also discussed in this chapter. The model was made based on the limited data available in open literature on Wilcox formation in the Gulf of Mexico to assure that it mimics an ultradeep, high pressure reservoir.

2.1 PVT Data

There are very limited publications on Wilcox formation in the Gulf of Mexico in open literature and, consequently, one of the major constraints on making the model for this study was lack of real data. **Tables 1 and 2** summarize the only useful data available on Wilcox formation in open literature which were used as the basis for making the model.

Table 1-Wilcox formation properties found in open literature

Reservoir Rock Data	
Permeability, md	0.3-30*
Average porosity, %	20
Rock type	sandstone

* Wilcox formation consists of similar layers (subdivisions). Permeability of each layer is typically less than 10 md and it degrades from 30 md on the top to 0.3 md at the bottom. Overal average permeability is about 5 md.

Table 2-Some other properties of Wilcox formation available in open literature

Reservoir PVT Data		General Reservoir Data	
Oil viscosity range, cp	1-10		
Initial average oil viscosity, cp	5	Water depth, ft	>5000
Average oil API gravity, °API	30.3	Reservoir depth, ft	25000-35000*
Gas specific gravity	0.7	Formation thickness, ft	700
Initial bubblepoint pressure, psia	1160.3	Initial Oil In Place, MMSTB	2000-5000
Initial reservoir pressure, psia	20300		
Initial solution gas/oil ratio, scf/STB	181.08 (<350)		
Reservoir temperature, °F	200		

* Below mud line (BML)

An initial black oil PVT table was first made using the oil and gas correlations given in Section 1.1 and the available data in Table 2. The following paragraphs explain step by step how the initial black oil table was made.

To make the initial black oil table, pseudo-reduced pressure and temperature of the reservoir fluid were first estimated using the given reservoir temperature and pressure in Table 2 and Standing correlations **(Eqs. 1.5 and 1.6).**

Gas deviation factor (Z-factor) was then estimated at pressures between standard pressure and initial reservoir pressure inclusive using Dranchuk and Abou-Kassem correlation **(Eq. 1.11).** Having done that, gas density and gas formation factor at each pressure were calculated using **Eqs. 1.12 and 1.14,** respectively**.**

Having gas density calculated, Lee-Gonzalez correlation (Eq. 1.15) was used to estimate gas viscosity at each pressure.

Wilcox oil is a low-GOR oil. Therefore, solution gas/oil ratio at pressures less than bubblepoint pressure was obtained by linear interpolation between standard conditions solution gas/oil ratio (0 scf/STB) and bubblepoint solution gas/oil ratio (181.08 scf/STB).

Having Wilcox oil viscosity at initial reservoir pressure, oil viscosity at bubblepoint pressure was back-calculated using Beal correlation **(Eq. 1.17).** The same correlation was then used to estimate other oil viscosities for undersaturated oil. After that, dead-oil viscosity was back-calculated using the estimated bubblepoint oil viscosity in the previous step and Chew and Connally correlation **(Eq. 1.18).** The same equation was used to estimate other oil viscosities for saturated oil. A_1 and A_2 parameters in Eq. 1.18 were obtained from Standing correlations given in **Eqs. 1.18a and 1.18b.**

Oil compressibility for undersaturated oil was estimated from Petrosky and Farshad correlation **(Eq. 1.19).** The estimated undersaturated oil compressibilities were comparable to estimated values from Vasquez and Beggs correlation (Eq. 1.20).

For estimation of bubblepoint oil formation volume factor, Petrosky and Farshad correlation **(Eq. 1.21)** was used. Having done that, linear interpolation was done between standard conditions oil formation volume factor (1 RB/STB) and bubblepoint oil formation volume factor. Then, Eq. 1.22 was used to calculate oil formation volume factor at undersaturated pressures.

Table 3 gives the initial black oil PVT table estimated for Wilcox oil through the aforementioned procedure.

The black oil PVT data given in Table 3 can be representative of different reservoir fluid compositions and equation-of-states (EOS). Therefore, it is not possible to estimate a unique fluid composition and its corresponding EOS from the initial black oil PVT table. On the other hand, black oil PVT table can only be used in simulation of recovery mechanisms in which reservoir fluid composition is not altered while for simulation of miscible CO_2 injection we needed to make a compositional model. Therefore, it was decided to consider one of the fluid compositions and EOS which can generate the initial black oil PVT table as the reservoir fluid composition and EOS for the compositional model.

Table 3-Initial black oil PVT table estimated from oil and gas correlations

Saturated Table

p_{sat} (psia)	B_o (RB/STB)	B_g (RB/scf)	R_s (scf/STB)	μ_o (cp)	μ_g (cp)
1160.3000	1.1342	0.0028	181.0800	2.2191	0.0147
1000.0000	1.1154	0.0032	155.7500	2.3591	0.0146
750.0000	1.0861	0.0044	116.2300	2.6091	0.0143
500.0000	1.0568	0.0067	76.7100	2.9077	0.0141
250.0000	1.0276	0.0133	37.1900	3.2706	0.0139
14.7000	1.0000	0.2368	0.0000	3.7312	0.0137

Undersaturated Table

P (psia)	B_o (RB/STB)	B_g (RB/scf)	μ_o (cp)	μ_g (cp)
2000	1.13243	0.00156	2.34110	0.01560
3000	1.13036	0.00105	2.48640	0.01670
4000	1.1283	0.00082	2.63170	0.01760
5000	1.12624	0.00070	2.77700	0.01840
6000	1.12419	0.00063	2.92230	0.01910
7000	1.12214	0.00058	3.06750	0.01960
8000	1.12009	0.00054	3.21280	0.02010
9000	1.11805	0.00052	3.35810	0.02050
10000	1.11601	0.00049	3.50340	0.02080
11000	1.11397	0.00048	3.64870	0.02120
12000	1.11194	0.00046	3.79400	0.02150
13000	1.10991	0.00045	3.93930	0.02170
14000	1.10789	0.00044	4.08460	0.02200
15000	1.10587	0.00043	4.22990	0.02220
16000	1.10385	0.00042	4.37520	0.02240
17000	1.10183	0.00041	4.52050	0.02260
18000	1.09983	0.00041	4.66580	0.02280
19000	1.09782	0.00040	4.81110	0.02300
20000	1.09582	0.00040	4.95640	0.02310
20300	1.09522	0.00039	5.00000	0.02320

To estimate a fluid composition and EOS for the reservoir fluid consistent with the initial black oil PVT table, we tried to tune the fluid composition and EOS parameters given by Killough and Kossack (1987) in the fifth SPE comparative solution project. The fluid composition and EOS used in the project is given in **Table 4.**

Table 4-Fluid composition and EOS used in the fifth SPE comparative solution project

Fluid Composition

Component	Mol%
C_1	50
C_3	3
C_6	7
C_{10}	20
C_{15}	15
C_{20}	5
Total	100

Equation-of-State Parameters

Component	p_c psia	T_c °R	M lb_m/lb_m mol	Parachore -	ω -	Z_c -
C_1	667.800	343.000	16.040	71.000	0.013	0.290
C_3	616.300	665.700	44.100	151.000	0.152	0.277
C_6	436.900	913.400	86.180	271.000	0.301	0.264
C_{10}	304.000	1111.800	142.290	431.000	0.489	0.257
C_{15}	200.000	1270.000	206.000	631.000	0.650	0.245
C_{20}	162.000	1380.000	282.000	831.000	0.850	0.235

As Wilcox oil is a low-GOR oil, the mole fraction of light components in the given fluid composition in Table 4 was decreased to be more consistent to that of Wilcox formation. Doing this, a reasonable match was obtained between Wilcox initial bubblepoint pressure (1160.3 psia) and our fluid initial bubblepoint pressure (1144.4 psia).

Volume shift for all the components were also added to the EOS given in Table 4 to match the resulting oil gravity to that of Wilcox oil (30.0 ^{o}API).

To get a match with Wilcox oil viscosity at initial reservoir pressure, critical Z-factors in the EOS in Table 4 were tuned. However, we did not manage to match the oil viscosities from the tuned EOS and those estimated in the initial black oil PVT table.

Table 5 gives the final fluid composition and EOS which was used for making the compositional model in this study.

Table 5-Final reservoir fluid composition and equation-of-state used for the model

Fluid Composition

Component	Mol%
CO_2	0.00000
N_2	0.00000
C_1	28.07430
C_3	4.31550
C_6	10.06960
C_{10}	28.77030
C_{15}	21.57770
C_{20}	7.19226
Total	100.00000

Equation-of-State Parameters

Component	p_c psia	T_c °R	M lbm/lbm mol	Parachore -	ω -	Z_c -	c_i -
CO_2	1069.51000	547.42000	44.01000	80.00000	0.22500	0.27433	0.00189
N_2	491.68000	227.29000	28.00000	59.10000	0.04000	0.29178	-0.16453
C_1	667.80000	343.00000	16.04000	71.00000	0.01300	0.29345	-0.15193
C_3	616.30000	665.70000	44.10000	151.00000	0.15240	0.27630	-0.06428
C_6	436.90000	913.40000	86.18000	241.83000	0.30070	0.25862	0.09681
C_{10}	304.00000	1111.80000	142.29000	376.50000	0.48850	0.23435	0.20911
C_{15}	200.00000	1270.00000	206.00000	529.40000	0.65000	0.19872	0.40916
C_{20}	162.00000	1380.00000	282.00000	711.80000	0.85000	0.20143	0.40155

Table 6 presents the black oil PVT table which is generated from the fluid composition and EOS given in Table 5 using the BLACKOIL keyword in SENSOR. The data file which generates this black oil table is presented in Appendix 2. This final black oil table which is consistent with fluid composition and EOS in Table 5, was used in the black oil runs of this study.

Table 6-Final reservoir black oil PVT table used for the model

Saturated Table

P_{sat} (psia)	B_o (RB/STB)	B_g (RB/scf)	R_s (scf/STB)	μ_o (cp)	μ_g (cp)
1144.40000	1.24480	0.00270	319.10000	0.71200	0.01410
1000.00000	1.22160	0.00311	273.70000	0.77400	0.01390
750.00000	1.18290	0.00417	198.60000	0.89200	0.01350
500.00000	1.14540	0.00639	127.00000	1.03000	0.01310
250.00000	1.10790	0.01299	57.40000	1.19700	0.01280
14.70000	1.07260	0.25250	0.00000	1.61200	0.01100

Undersaturated Table

P (psia)	B_o (RB/STB)	B_g (RB/scf)	μ_o (cp)	μ_g (cp)
1500.3	1.2336	0.00204	0.7820	0.01480
2000.0	1.2195	0.00152	0.8830	0.01600
2500.6	1.2071	0.00122	0.9860	0.01740
2800.1	1.2003	0.0011	1.0490	0.01840
4000.0	1.1773	0.00081	1.3090	0.02250
5000.0	1.1617	0.00068	1.5320	0.02590
6000.0	1.1485	0.00061	1.7610	0.02910
7000.0	1.1371	0.00055	1.9920	0.03200
8000.0	1.1272	0.00052	2.2250	0.03470
9000.0	1.1185	0.00049	2.4600	0.03740
10000.0	1.1107	0.00046	2.6950	0.03990
12000.0	1.0974	0.00043	3.1610	0.04500
13000.0	1.0917	0.00042	3.3930	0.04750
14000.0	1.0865	0.00041	3.6220	0.05000
16000.0	1.0773	0.00039	4.0720	0.05520
17000.0	1.0732	0.00038	4.2930	0.05780
18000.0	1.0694	0.00037	4.5110	0.06050
19000.0	1.0659	0.00037	4.7260	0.06320
20300.0	1.0616	0.00036	5.0000	0.06680

Figures 3 to 7 illustrate the comparison between the initial and final black oil PVT table parameters. The parameters in the initial black oil PVT table were estimated using oil and gas correlations and the ones in the final black oil PVT table were obtained from the EOS and fluid composition presented in Table 5.

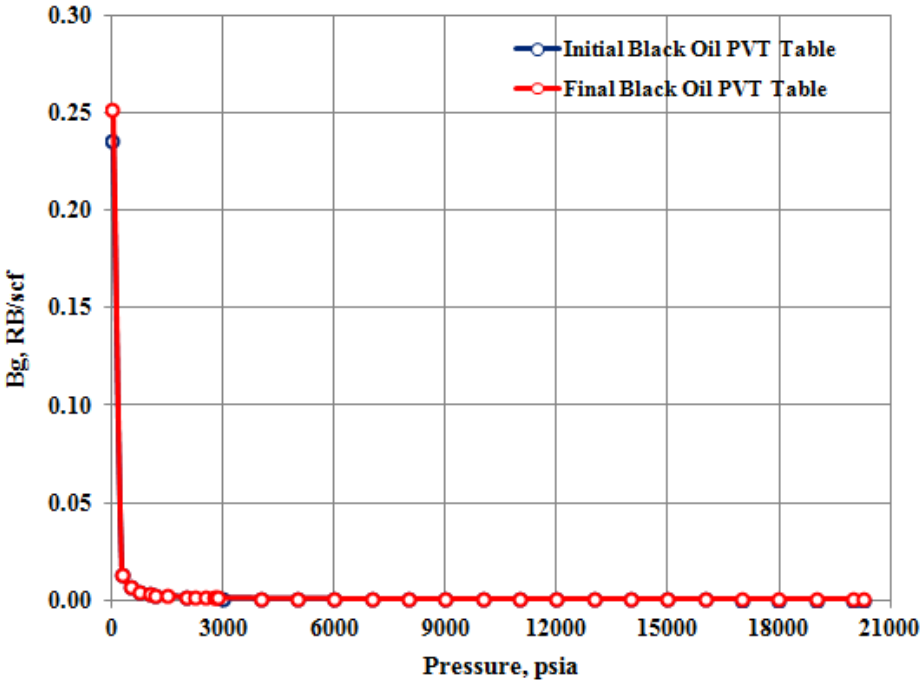

Figure 3-Gas formation volume factor from the initial and final black oil PVT tables

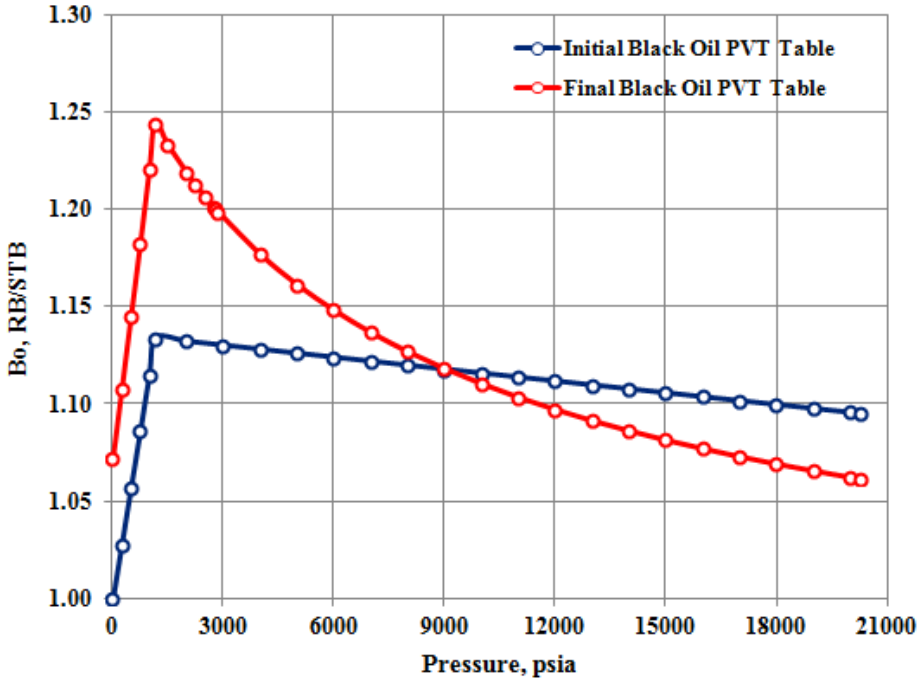

Figure 4-Oil formation volume factor from the initial and final black oil PVT tables: a reasonable match for initial bubblepoint pressure

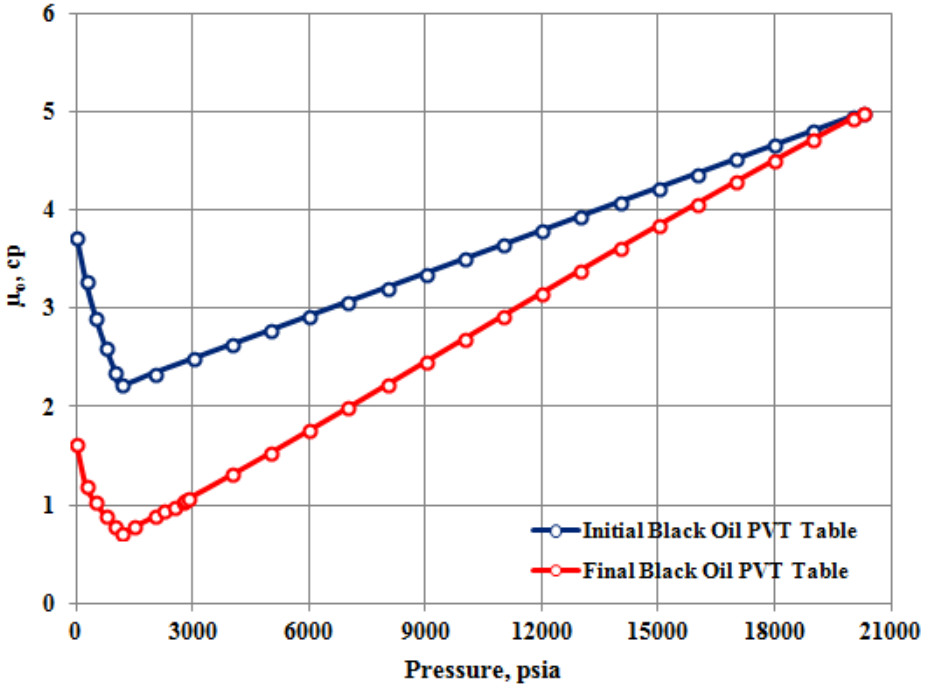

Figure 5-Oil viscosity factor from the initial and final black oil PVT tables: a perfect match for oil viscosity at initial reservoir pressure

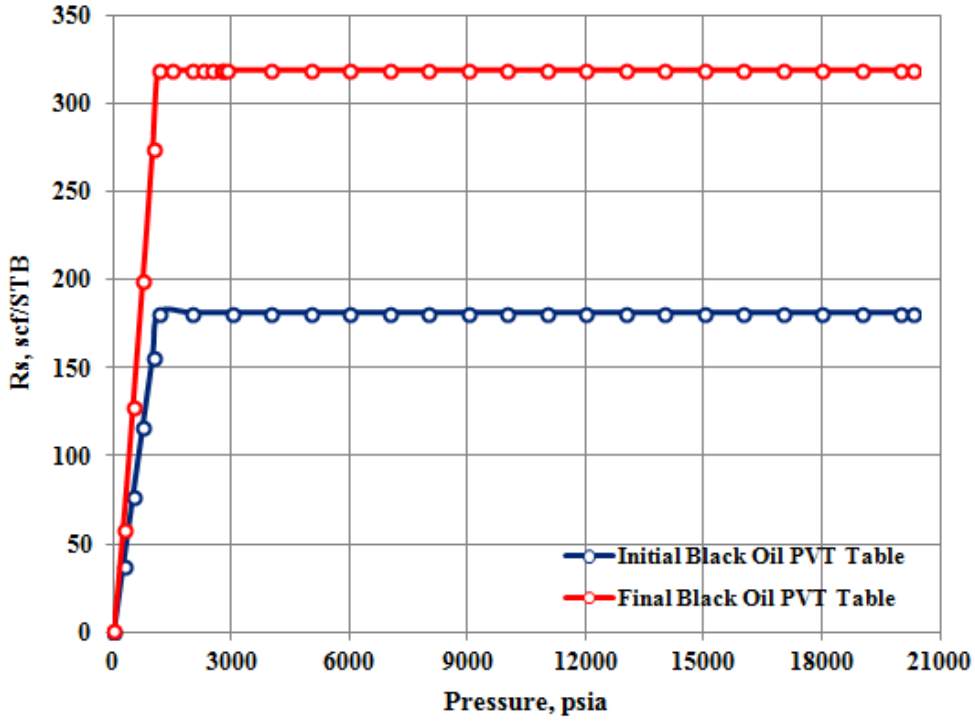

Figure 6-Solution gas/oil ratio from the initial and final black oil PVT tables

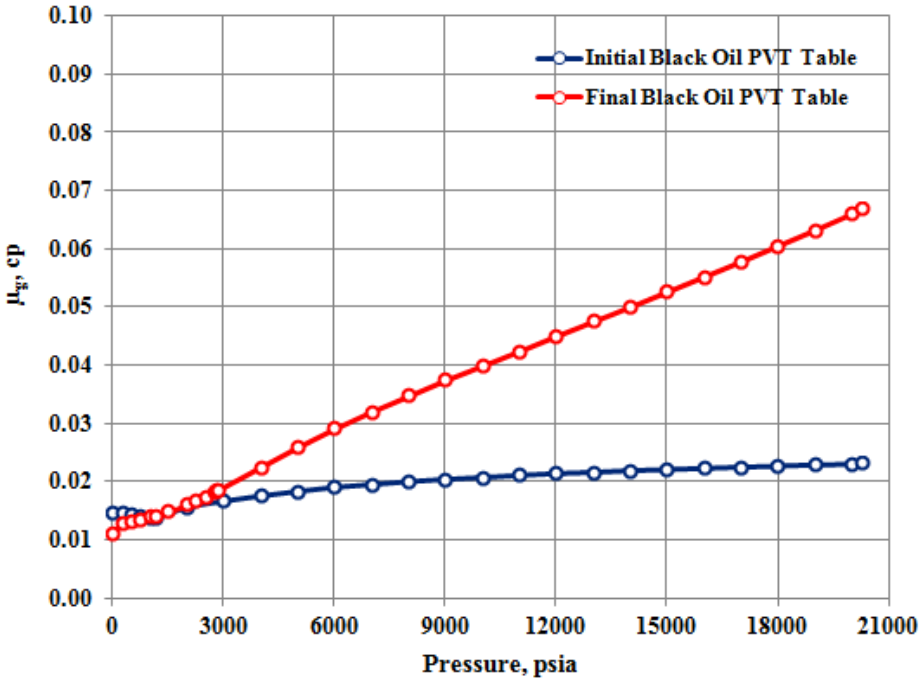

Figure 7-Gas viscosity from the initial and final black oil PVT tables

2.2 Grid Model

Another problem in making the model was constraint on the maximum possible number of grid cells (6000) in SENSOR. This could result in a very course-grid model which, in consequence, would possibly yield erroneous simulation results due to numerical dispersion. To reduce the effect of numerical dispersion, one-twentieths of the main cubic reservoir grid model was selected for the simulation study. To do this the reservoir area for the main cubic reservoir containing the same volume of oil as initially found in Wilcox formation was calculated using **Eq. 2.1**.

$$\text{OOIP} = Ah\varphi\frac{(1-S_{wi})}{5.615B_{oi}} \tag{2.1}$$

in which h is reservoir thickness in ft, A is reservoir area in ft^2, B_{oi} is in RB/STB, and original oil in place (OOIP) is in STB.

As shown below, using an average OOIP of 3000 MMSTB and an assumed initial average water saturation of 0.2 gave a reservoir area of 1.59667×10^8 ft^2.

$$A = \frac{3x10^9 \text{ x } 1.0616}{0.17809 \text{ x } 140 \text{ x } 0.2 \text{ x } (1\text{-}0.2)} = 1.59667x10^8 \ (ft^2)$$

On the basis of symmetrical cubic reservoir and considering the fact that Wilcox formation consists of repetitive layers (see Table 1), a cubic section of the reservoir was selected as the

final model for the simulation study. The selected section was then discretized to 24x24 uniform numerical grids in *XY* plane and 10 nonuniform numerical grids in *Z* direction. **Table 7** gives the dimensions of the selected section and the corresponding grid blocks.

Table 7- Dimensions of the selected section of the cubic Wilcox reservoir model

		Grid Block	Thickness, ft
OOIP, STB	$3x10^9/20=1.5x10^8$	1	8.86
Reservoir thickness,ft	700/5=140	2	7.80
Reservoir area, ft^2	$1.59667x10^8/4=3.99166x10^7$	3	3.80
NX	24	4	3.50
NY	24	5	4.10
NZ	10	6	9.80
DX, ft	263.25	7	12.74
DY, ft	263.25	8	1.13
		9	14.27
		10	74.00
		Total	140.00

Figure 8 also illustrates the final grid model the dimensions of which are given in Table 7. As shown in Table 7 and Fig. 8, the final grid model, which was used in this study, is a cubic model which is one-twentieth of the main cubic reservoir model in volume. It has an area equal to a quarter of the area of the main reservoir model and a thickness equal to one-fifth of the thickness of the main reservoir model.

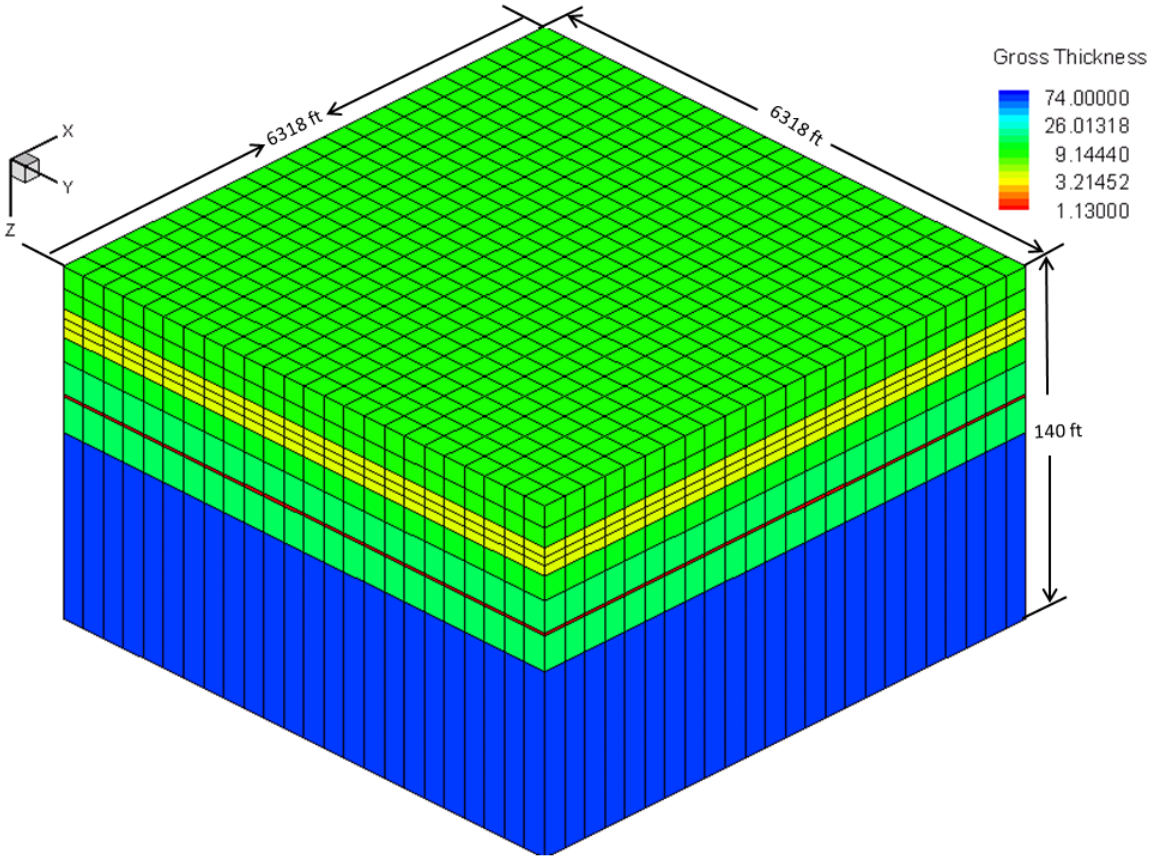

Figure 8-Final reservoir section grid model

As shown in **Table 8**, the 10 grid blocks in Z direction in the final grid model are grouped in to three layers. The first layer from top is made up of the first three grid blocks, the second layer consists of the next four grid blocks, and the last three grid blocks make up the last layer at the bottom. Permeability in each layer is distributed in the constituting grid blocks in a manner that is consistent with permeability distribution in the individual layers and the overall average permeability in Wilcox formation as shown in Table 1.

The data used for model equilibration (initialization) are given in **Table 9.** Due to lack of data on Wilcox formation, some of these data (water properties, initial water saturation, and rock compressibility) were taken from available typical data in the literature. Also, a water depth of 2500 m SSTVD and a reservoir depth of 10,000 m SSTVD for the model were assumed. These values are within the ranges of those of Wilcox formation in the Gulf of Mexico.

Table 8- Permeability distribution in the final grid model

	$k_x=k_y$, md	Thickness, ft	Grid Block
Layer 1	30.00	8.86	1
	19.30	7.80	2
	0.30	3.80	3
Layer 2	30.00	3.50	4
	8.90	4.10	5
	4.00	9.80	6
	0.30	12.74	7
Layer 3	30.00	1.13	8
	2.95	14.27	9
	0.30	74.00	10

Overal average permeability=$\sum k_i h_i / \sum h_i$=5 md

$k_z=0.1(k_x k_y)^{0.5}$

Table 9- Data used for model initialization

Reservoir Grid and Saturation Input Data	
Datum (from sea floor), ft	24606
No gas/oil contact and water/oil contact	
Initial reservoir pressure, psia	20300
Initial water saturation, %	20
Porosity (at initial reservoir pressure), %	20
Initial saturation pressure, psia	1144.4
Water properties	
Density, lb/ft^3	62.4
Compressibility, 1/psi	3×10^{-6}
Rock pore volume compressibility, 1/psi	1×10^{-6}

2.3 Relative Permeability and Capillary Pressure Curves

Due to lack of relative permeability data, we had to use analytical k_r data. **Table 10** gives the values used for analytical k_r calculations.

Table 10- Variables used for analytical k_r calculations in the model

Variable	Used Value
S_{wc}	0.20
S_{orw}	0.20
S_{org}	0.00
S_{gc}	0.00
k_{rwro}	1.00
k_{rgro}	0.99
k_{rocw}	0.99
n_w	2.00
n_{ow}	2.00
n_g	2.00
n_{og}	2.00

Figures 9 and 10 illustrate the calculated analytical relative permeability curves by SENSOR using the variables given in Table 10.

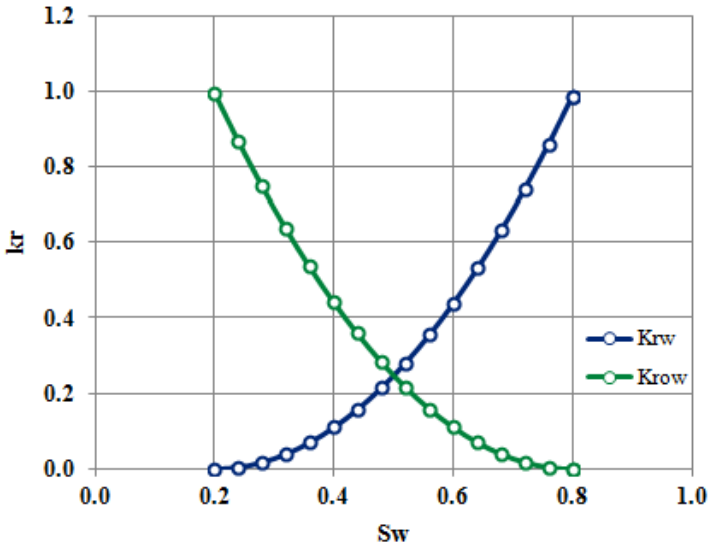

Figure 9-Analytical oil/water relative permeability curves generated by SENSOR

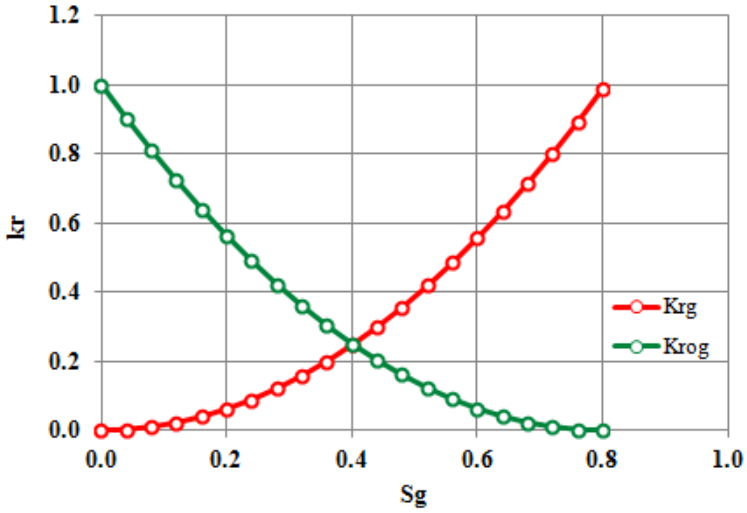

Figure 10- Analytical oil/gas relative permeability curves generated by SENSOR

Zero capillary forces were assumed for the model under study.

2.4 Well Data

All layers were perforated in the producer(s) and injector(s) and the default well radius in SENSOR (0.25 ft) was considered for the wellbores. To be consistent with the typical bottomhole pressures in Wilcox formation in the Gulf of Mexico, a minimum bottomhole peressur of 8000 pasi for producer(s) and a maximum injection pressure of 15000 psia for injector(s) were considered for the wells in the model. Very high production and injection rates were considered in the model to set the production and injection constratints on the minimum bottomhole pressure in producer(s) and maximum injection pressure in injector(s).

Well indexes (productivity index and injectivity index) in each layer was calculated using Peacemen's formula.

Table 11 summarizes the well data used in the final model.

Table 11-Well data in the final model

Production Well Data		Layer	Productivity Index (RB.cp)/(d.psi)
Perforations K=1-10 (all layers)			
Radius, ft	0.25	1	1.248
Minimum bottomhole pressure, psia	8000	2	0.803
Maximum production rate, STB	1×10^{10}	3	0.012
		4	1.248
Injection Well Data		5	0.370
		6	0.166
Perforations K=1-10 (all layers)		7	0.012
Radius, ft	0.25	8	1.248
Maximum injection pressure, psia	15000	9	0.123
Maximum injection rate, MMscf	1×10^{10}	10	0.012

Chapter 3: Optimization Strategy

Through this study, we tried to demonstrate how optimization of well placement, inter-well spacing, and EOR startup time can maximize ultimate and incremental oil productions in an ultradeep, high pressure oil reservoir.

Ultimate oil recovery resulting from depletion of the ultradeep, high pressure oil reservoir in this study followed by miscible CO_2 injection is a function of numerous parameters which include but are not limited to injection pressure, BHP, number of wells, injection and production schemes, inter-well spacing, well placement (well location), CO_2 injection startup time, well completion, etc. Of these parameters, considering the objective of this study, number of wells, well placement, inter-well spacing, and CO_2 startup time were taken as variables. All other parameters in the model were set as explained in Chapter 2.

The optimization strategy employed in the study consists of two main steps:

1) Determining the maximum ultimate oil recovery (R_{EOR}) from pressure depletion of the reservoir followed by miscible CO_2 flooding by finding the optimum CO_2 injection startup time (t_D) and well spacing: This was done for different well patterns (2-spot, 3-spot, 4-spot, and 5-spot) to account for different well placements and number of wells. Therefore, the variables for each well pattern were only t_D and well spacing. We assumed that 1000 STB of oil production was the economic criteria for end of simulation run (t_{EOR}) for each well pattern scenario.

2) Determining the maximum incremental oil recovery (ΔR) for the optimum t_D and well spacing defined in the previous step: To do this, first, ultimate oil recovery (R_D) from depletion of the reservoir was determined for the optimum well spacing and over t_{EOR} defined in the previous step. Then, ΔR was determined using **Eq. 3.1.**

$$\Delta R = R_{EOR} - R_D \tag{3.1}$$

Chapter 4: Results and Discussions

4.1 MMP Estimation for CO_2 Miscible Injection

In miscible gas injection, injection pressure should be sufficiently more than the MMP estimated for the reservoir fluid system and injected gas.

The estimated MMP by PhazeComp, which is an EOS-based program, for our reservoir fluid and CO_2 as the injectant was 2499 psia. The estimated MMP is much lower than the maximum injection pressure of 15000 psia set in the model and, thus, CO_2 injection was miscible throughout the EOR phase. However, we used the first-contact miscibility option in SENSOR by using the OIL keyword and setting p_{sat} equal to zero in the model to make sure that our displacement mechanism is fully miscible.

The PhazeComp data file used for MMP estimation is given in Appendix 3.

4.2 Well Spacing and t_D Optimization for 2-Spot Well Pattern

In the 2-spot well pattern both wells produced for a while and one of the producers (well 2) was then converted to CO_2 injector till end of CO_2 injection, where economic limit of 1000 STB of oil production was approached.

Figure 11 shows the plan view of the final grid model. As clear from the figure, the 2-wells in the model can be placed in thousands of positions with respect to each other and each position results in a specific cumulative oil production at t_{EOR} for a given t_D. To reduce the number of simulation runs in the simulation process, first, we did a sensitivity analysis on the effect of moving the wellbore positions from center of the model to the corners and boundaries of the model on cumulative oil production. To do this, cumulative oil production after 20 years of pressure depletion of the reservoir for different well spacings along AA′, BB′, and CC′ lines shown in **Fig. 12** were compared**.** Similar comparison was done for different well spacings along DD′, EE′, FF′, and GG′ lines shown in **Fig. 13.**

Figure 14 shows cumulative oil productions after 20 years of pressure depletion of the reservoir for all possible well spacings along AA′, BB′, and CC′ lines. As clear from the figure, maximum cumulative oil production was observed along AA′ line where producer 1 was on *i*=6 and producer 2 was located on *i*=18. Furthermore, the maximum cumulative oil production decreased as we moved the wells from AA′ line to BB′ line and from BB′ line to CC′ line. In other terms, as we moved the wells from the center of the model to the boundaries of the model, maximum cumulative oil production decreased. The same behavior was observed in pressure depletion of the reservoir followed by CO_2 miscible injection.

Figure 15 illustrates cumulative oil productions after 20 years of pressure depletion of the reservoir for all possible well spacings along DD′, EE′, FF′, and GG′ lines. We observed the maximum cumulative oil production along DD′ line where producer 1 was on *i*=8 and producer 2 was located on *i*=17. Furthermore, the maximum cumulative oil production decreased as we moved the wells from DD′ line to EE′ line, from EE′ line to FF′ line, and from FF′ line to GG′ line. In other terms, as we moved the wells from the center of the model to the corners of the model, maximum cumulative oil production decreased. The same behavior was observed in pressure depletion of the reservoir followed by CO_2 miscible injection.

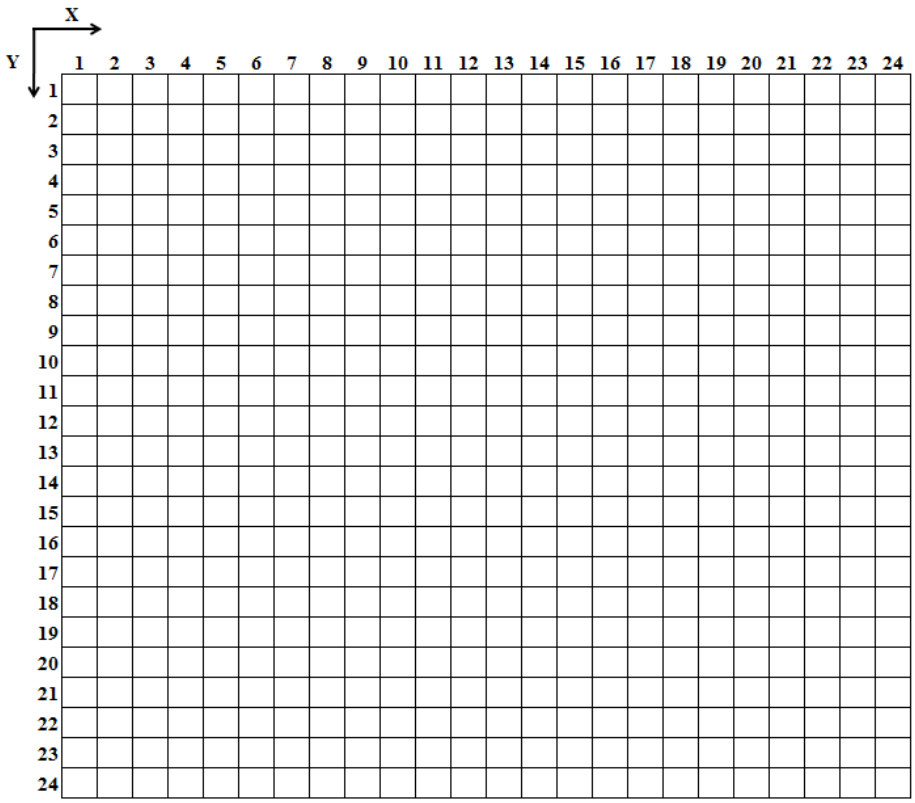

Figure 11-Plan view of the final grid model

Based on the observations made in the sensitivity analysis (Figs. 14 and 15), to reduce the number of simulation runs in the optimization process, we went through the two steps of the optimization process, explained in Chapter 3, along AA′ and DD′ lines. The optimization

process for the 2-spot well pattern along AA′and DD′lines consisting of 1663 simulation runs found the optimum t_D and well spacing along DD′ given in **Table 12.**

Table 12-Optimum well locations and EOR startup time for 2-spot well pattern

Optimum Well Locations (I,J)		Optimum t_D, years
Well 1	Well 2	5.2
(9,16)	(16,9)	

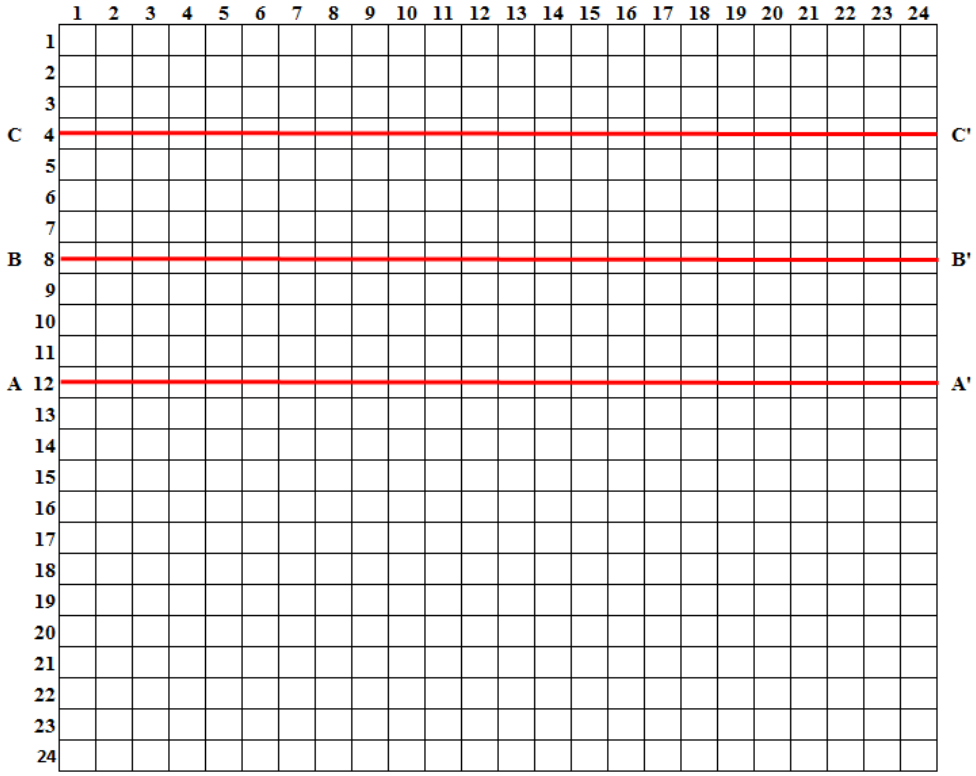

Figure 12-Moving well positions to the boundaries of the model

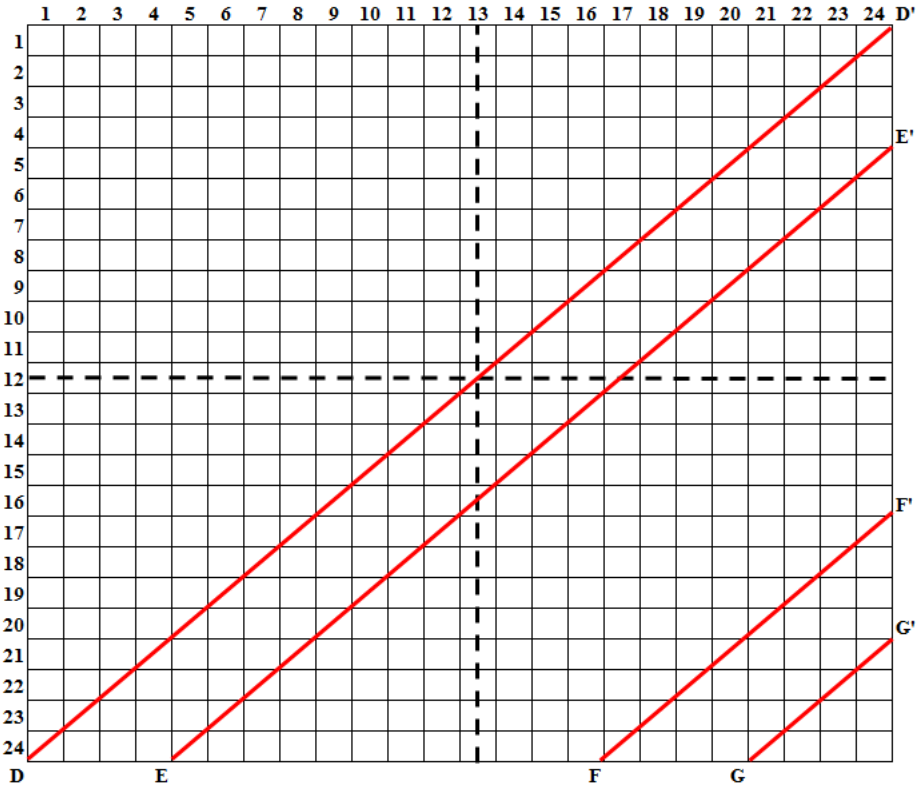

Figure 13-Moving well positions to the corners of the model

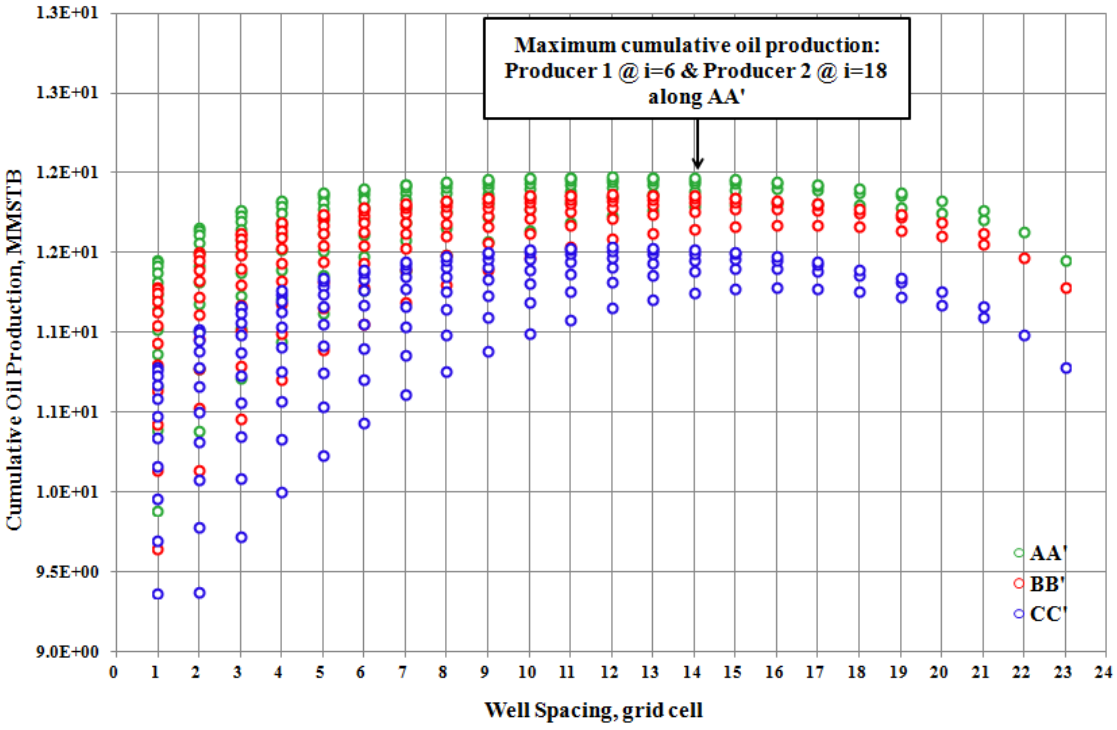

Figure 14-Cumulative oil productions after 20 years of pressure depletion for different 2-spot well spacings along AA', BB', and CC' lines

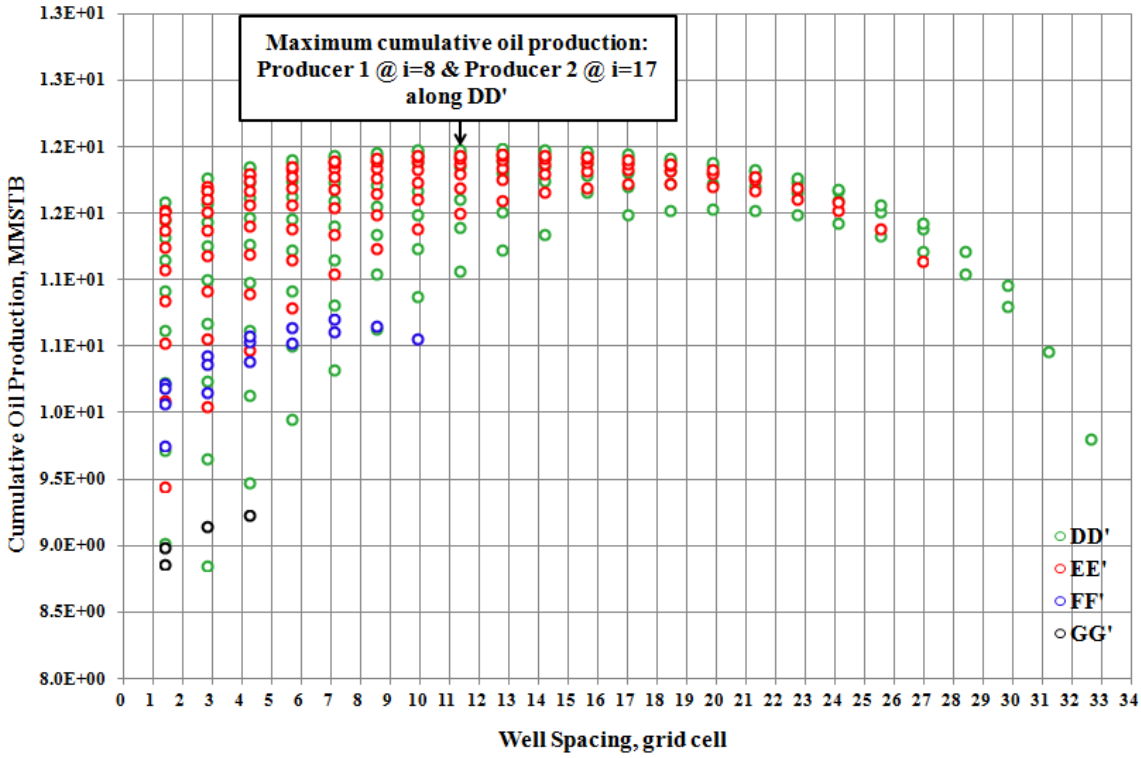

Figure 15- Cumulative oil production after 20 years of pressure depletion for different 2-spot well spacings along DD′, EE′, FF′, and GG′ lines

Well 2 was converted to an injector after 5.2 years of production and CO_2 injection continued up to 63.84 years (t_{EOR}) where the economic limit of 1000 STB of oil production was reached. This optimum t_D and well spacing gave a maximum cumulative oil recovery of 44.876 MMSTB which is equivalent to an oil recovery of 29.9% over t_{EOR}.

Figure 16 compares the oil recovery from the optimum t_D (5.2 years) and well spacing with those from the same well spacing but later CO_2 injection startup times.

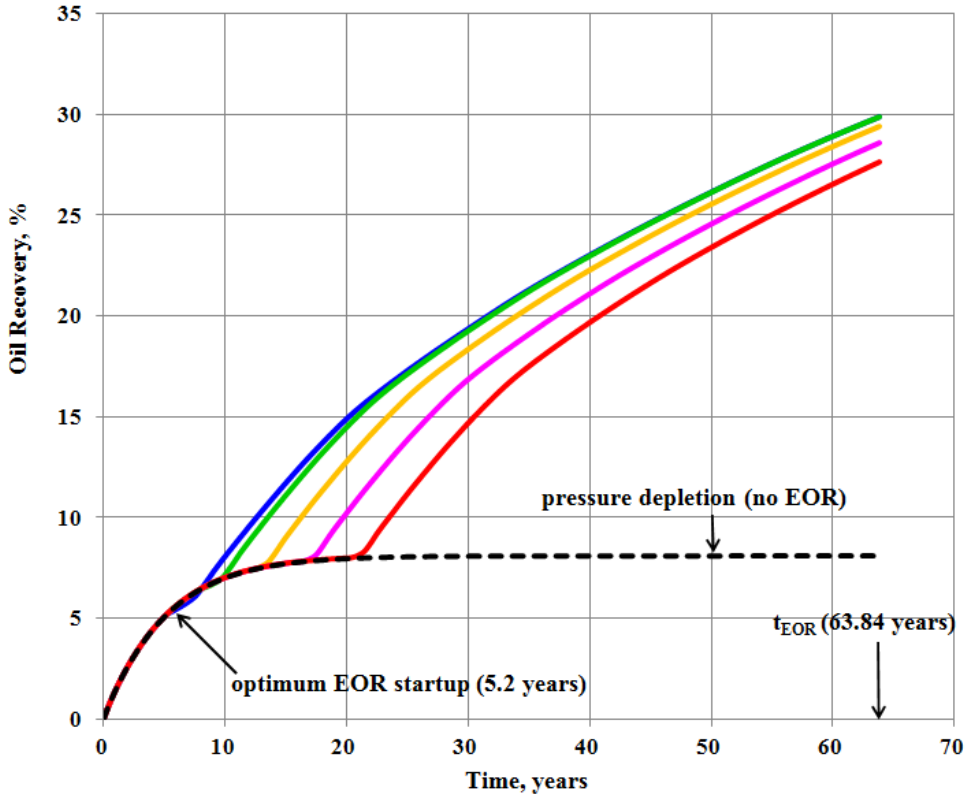

Figure 16-Comparison between recoveries from optimum t_D and those from other t_D's over t_{EOR} for a 2-spot well pattern

According to **Fig. 17** higher oil production rate is maintained for a longer time in the case of the optimum t_D which in consequence results in maximized cumulative oil production over t_{EOR}.

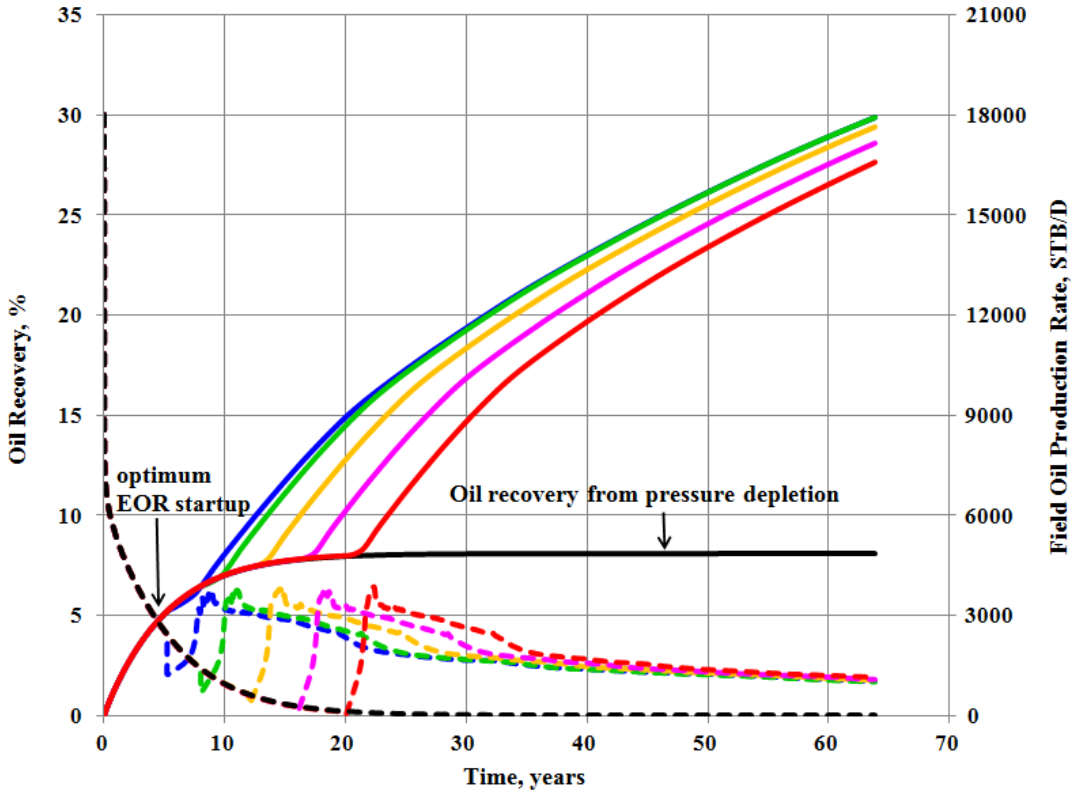

Figure 17-Effect of EOR startup time on oil production rate and oil recovery

Figs. 18, 19, and 20 demonstrate pressure distribution at optimum t_D in grid blocks 1, 2, and 3 of layer 1, respectively. It is clear from these figures that no high pressure isolation region was left after pressure depletion of these layers regardless of the permeability of these layers. Similar uniform pressure distribution was observed in all grid blocks of the other 2 layers in the model regardless of their permeability (see Table 8).

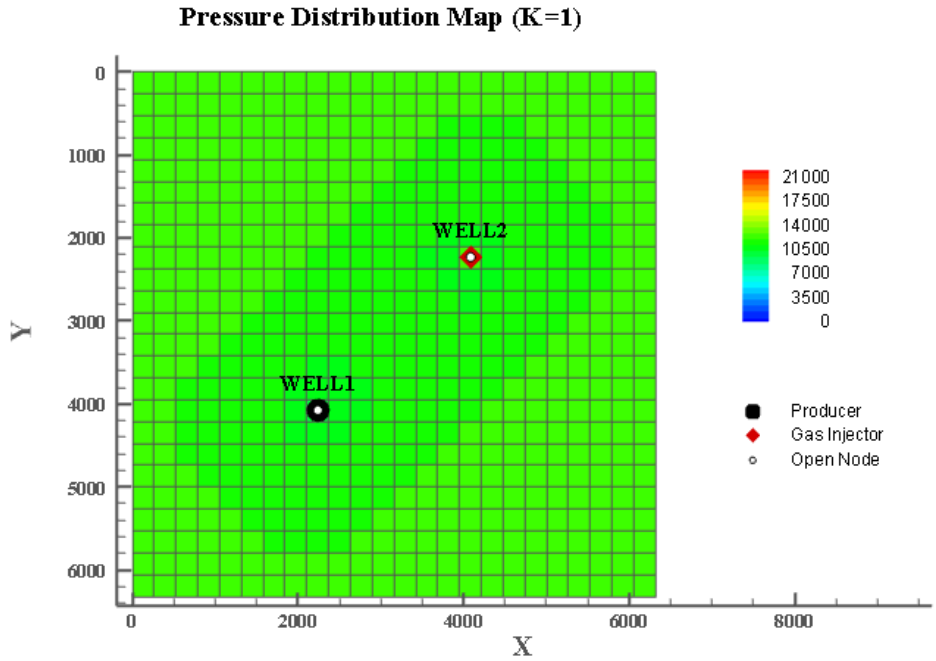

Figure 18-Uniform pressure distribution in grid block 1 of layer 1 with k=30 md at optimum t_D and for optimum well spacing

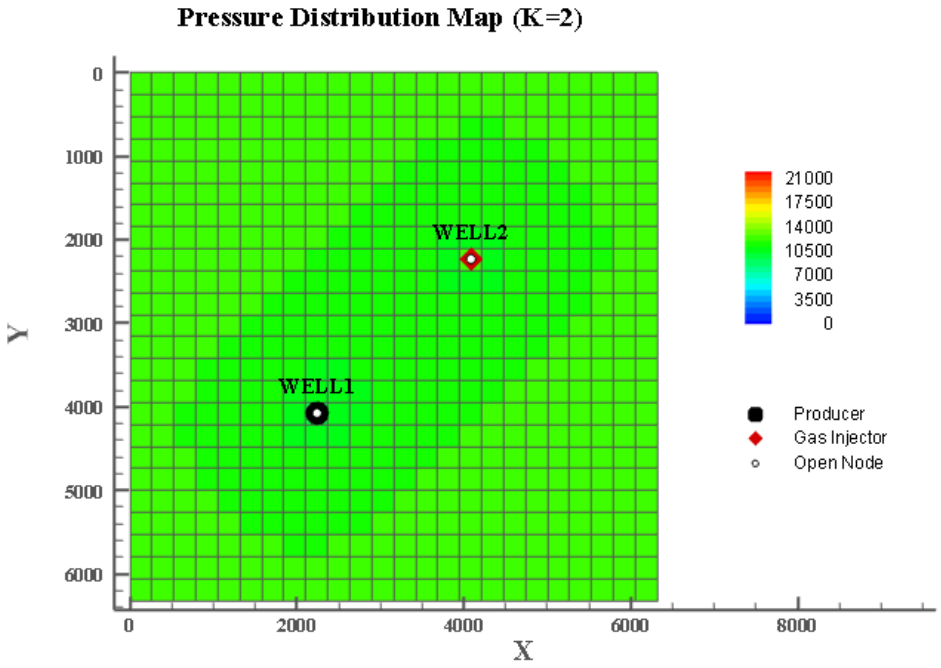

Figure 19- Uniform pressure distribution in grid block 2 of layer 1 with k=19 md at optimum t_D and for optimum well spacing

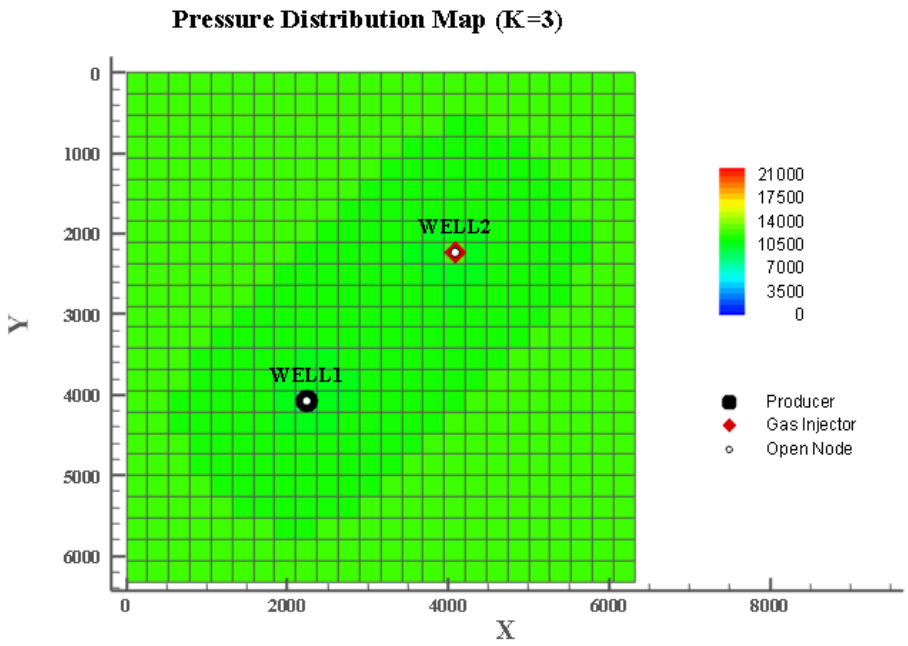

Figure 20- Uniform pressure distribution in grid block 3 of layer 1with k=0.3 md at optimum t_D and for optimum well spacing

4.3 Well Spacing and t_D Optimization for 3-Spot Well Pattern

In the 3-spot well pattern analysis, producer 2 which was converted to an injector at t_D was placed on grid cell (13,12) throughout the simulation run and the other two wells were relocated through optimization process to find the optimum well spacing and t_D.

Similar sensitivity analysis that we did for the 2-spot well pattern was performed for the 3-spot well pattern to reduce the number of simulation runs and the same conclusions were drawn. That is, while keeping producer 2 at grid number (13,12), moving producer 1 and 3 from the center of the model to the boundaries and corners of the model resulted in decrease in cumulative oil production. Therefore, like the 2-spot well pattern, we conducted the optimization process along AA′ and DD′ lines consisting of 1099 simulation runs. The found optimum t_D and well spacing, which was along AA′, are given in **Table 13.**

Table 13- Optimum well locations and EOR startup time for 3-spot well pattern

Optimum Well Locations (I,J)			Optimum t_D, years
Well 1	Well 2	Well 3	3.15
(2,12)	(13,12)	(23,12)	

Well 2 was converted to CO_2 I injector after 3.15 years of production and CO_2 injection continued up to 59.31 years (t_{EOR}) where the economic limit of 1000 STB of oil production was reached. This optimum t_D and well spacing gave a maximum cumulative oil recovery of 57.443 MMSTB which is equivalent to an oil recovery of 38.29% over t_{EOR}.

Figure 21 compares the oil recovery from the optimum t_D (3.15 years) and well spacing with those from the same well spacing but later CO_2 injection startup times.

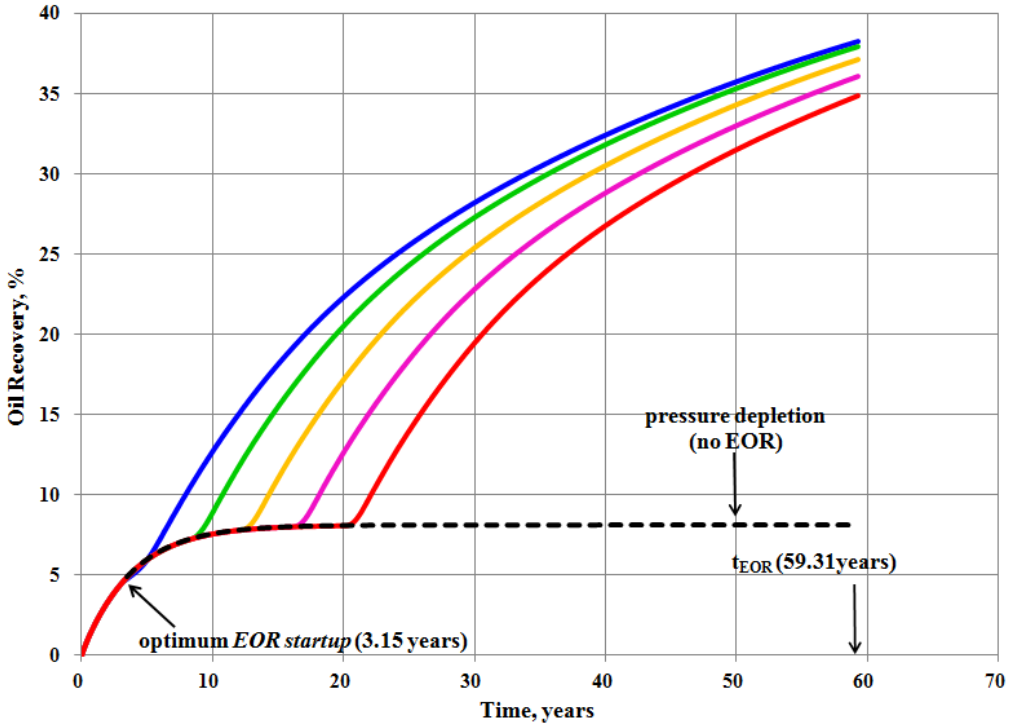

Figure 21-Comparison between recoveries from optimum t_D and those from other t_D's over t_{EOR} for a 3-spot well pattern

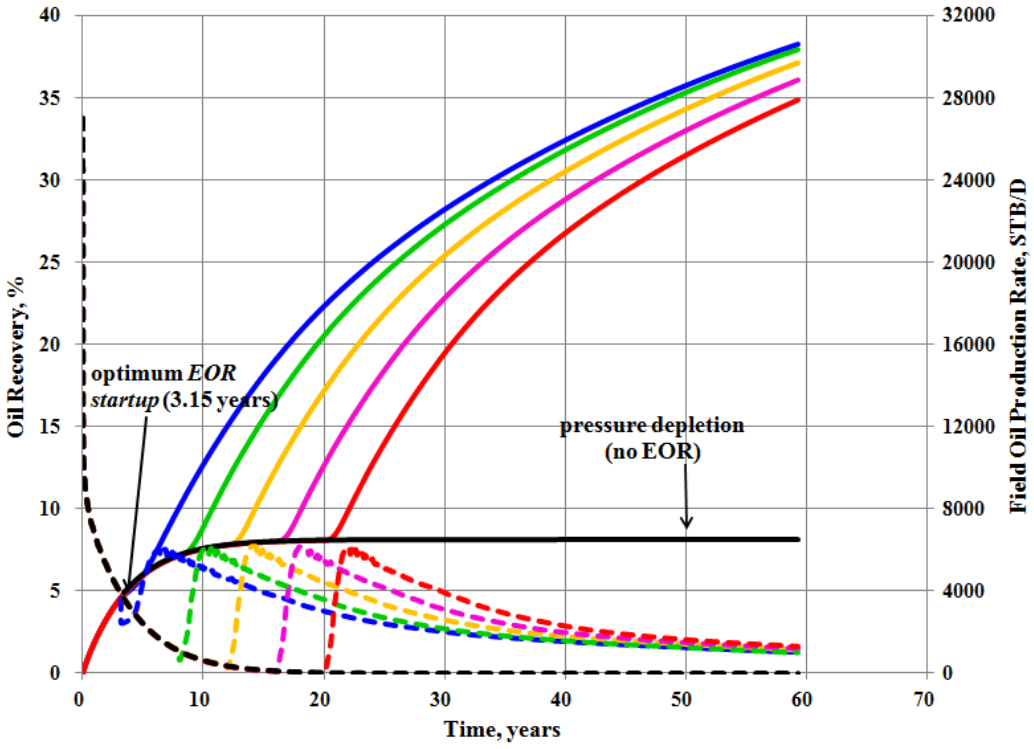

Figure 22-Effect of EOR startup time on oil production rate and oil recovery

As shown in **Fig. 22,** higher oil production rate is maintained for a longer time in the case of the optimum t_D which in consequence results in maximized cumulative oil production over t_{EOR}.

Similar to the case of optimum 2-spot well pattern, for the case of optimum 3-spot well pattern, uniform pressure distribution was observed at t_D in all grid blocks of the 3 layers in the model regardless of their permeability. This is shown for the 3 grid blocks of layer 1 in **Figs. 23, 24, and 25.**

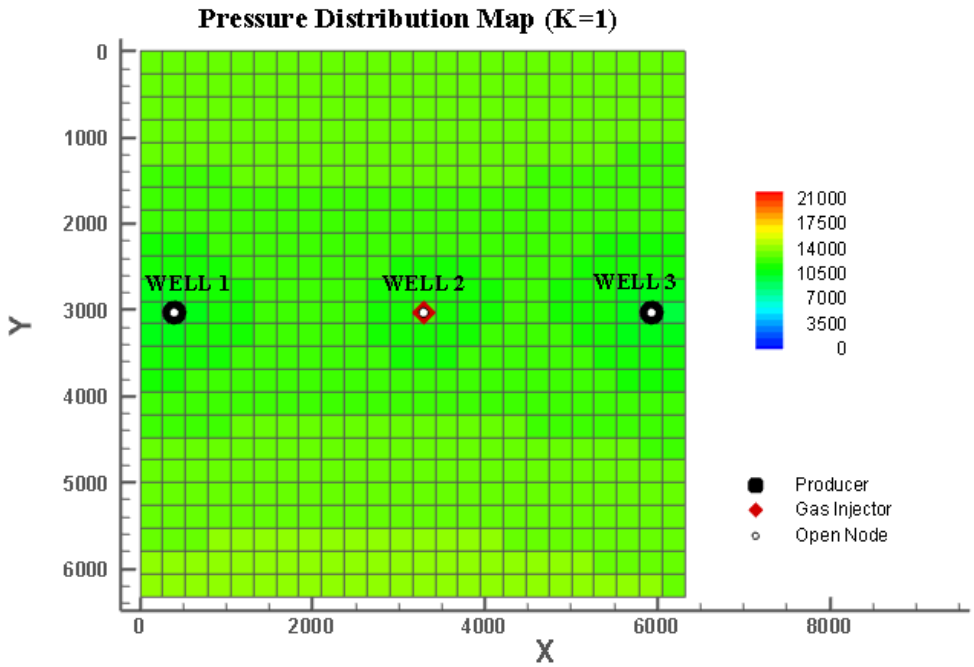

Figure 23-Uniform pressure distribution in grid block 1 of layer 1 with k=30 md at optimum t_D and for optimum well spacing

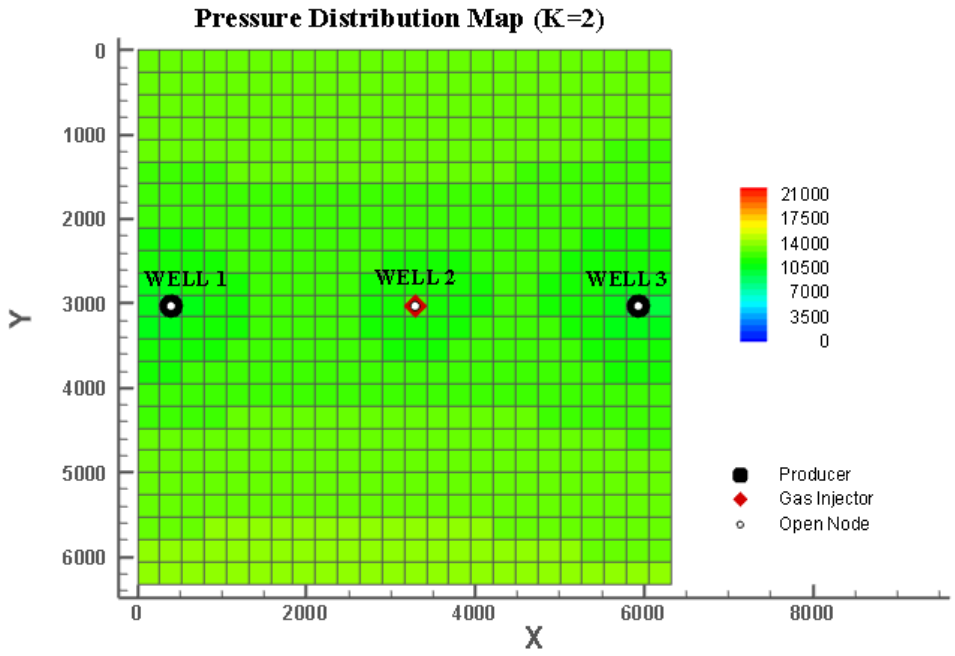

Figure 24-Uniform pressure distribution in grid block 2 of layer 1 with k=19 md at optimum t_D and for optimum well spacing

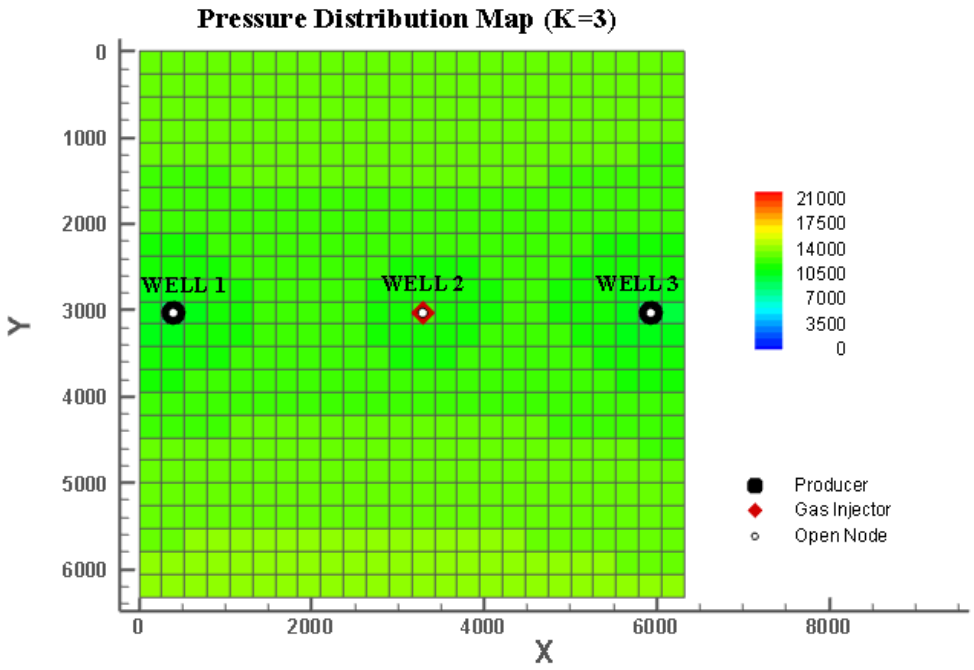

Figure 25-Uniform pressure distribution in grid block 3 of layer 1 with k=0.3 md at optimum t_D and for optimum well spacing

4.4 Well Spacing and t_D Optimization for 4-Spot Well Pattern

In the 4-spot well pattern, 3 wells (wells 1, 3, and 4) were located on the 3 vertices of a triangle and the 4th well (well 2) was placed at the center of the triangle. Well 2 was permanently positioned at the center of the triangle while the other 3 well on the vertices of

the triangle were moved uniformly away from well 2 through the optimization process to find the optimum well spacing for the 4-spot well pattern. Sensitivity to t_D was also done for each 4-spot well pattern to find the optimum t_D.

Before the optimization process, similar sensitivity analysis to that in the case of 2-spot and 3-spot well patterns was done to investigate the effect of moving the wells in the model to the boundaries and corners of the model on cumulative oil production. To do this, well 2 at the center of the 4-spot well pattern was moved along AA′, CC′, DD′, and EE′ lines **(Fig. 26)** and the cumulative oil production for a 20-year pressure depletion for all the possible 4-spot well patterns along these lines were obtained and compared **(Fig. 27)**.

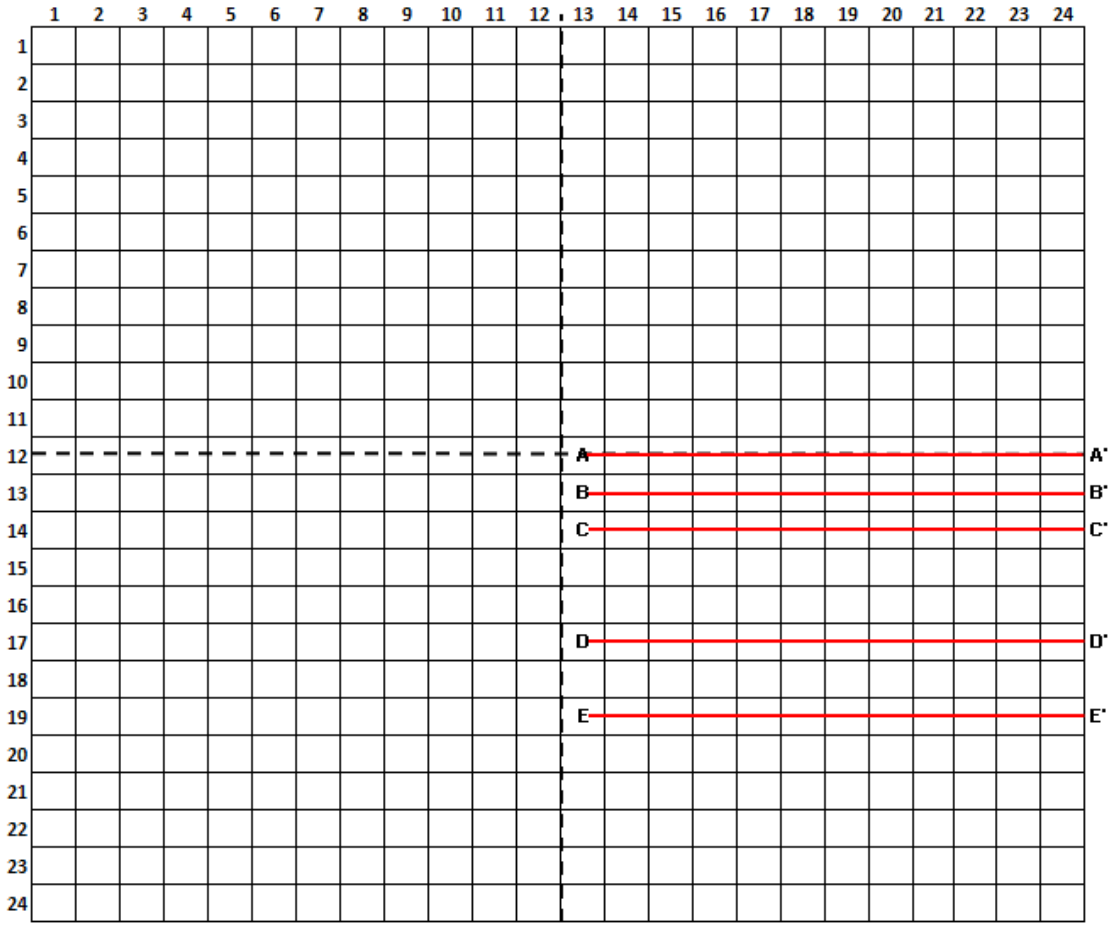

Figure 26-Moving well positions to the boundaries and corners of the model

As shown in Fig. 27, moving the wells to the boundaries and corners of the reservoir resulted in reduction in cumulative oil production. The same behavior was observed for the case of pressure depletion of the reservoir followed by miscible CO_2 injection.

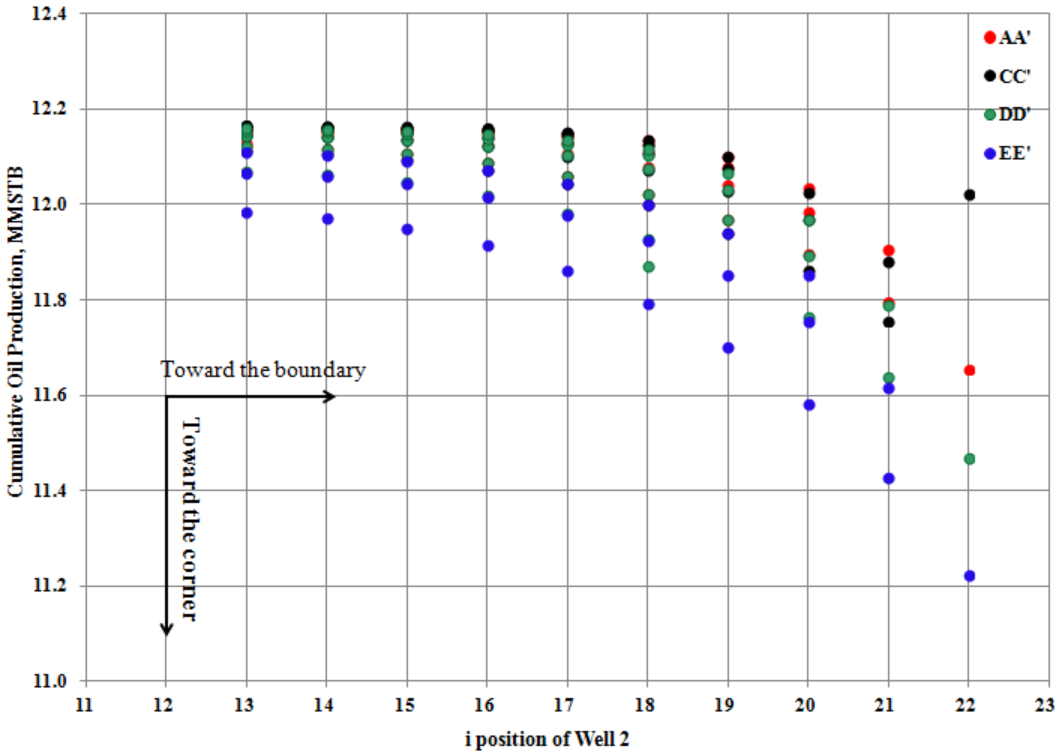

Figure 27-Cumulative oil production after 20 years of pressure depletion for different 4-spot well spacings along AA′, CC′, DD′, and EE′ lines

Based on the results of the sensitivity analysis, optimization process was performed for all possible 4-spot well patterns along AA′, BB′, and CC′ lines**. Table 14** gives the optimum well spacing and t_D found in optimization of the 4-spot well pattern consisting of 525 simulation runs. These optimum parameters gave maximum cumulative oil production of 62.045 MMSTB over t_{EOR} of 54.11 years which is equivalent to an oil recovery of 41.36%.

Table 14- Optimum well locations and EOR startup time for 4-spot well pattern

Optimum Well Locations (I,J)				Optimum t_D, years
Well 1	Well 2	Well 3	Well 4	2
(5,5)	(13,13)	(21,5)	(13,22)	

Figure 28 compares the oil recovery from the optimum t_D (2 years) and well spacing with those from the same well spacing but later CO_2 injection startup times.

Similar to 2-spot and 3 spot well pattern scenarios, as shown in **Fig. 29,** for the 4-spot well pattern, higher oil production rate is maintained for a longer time in the case of the optimum t_D which in consequence results in maximized cumulative oil production over t_{EOR}.

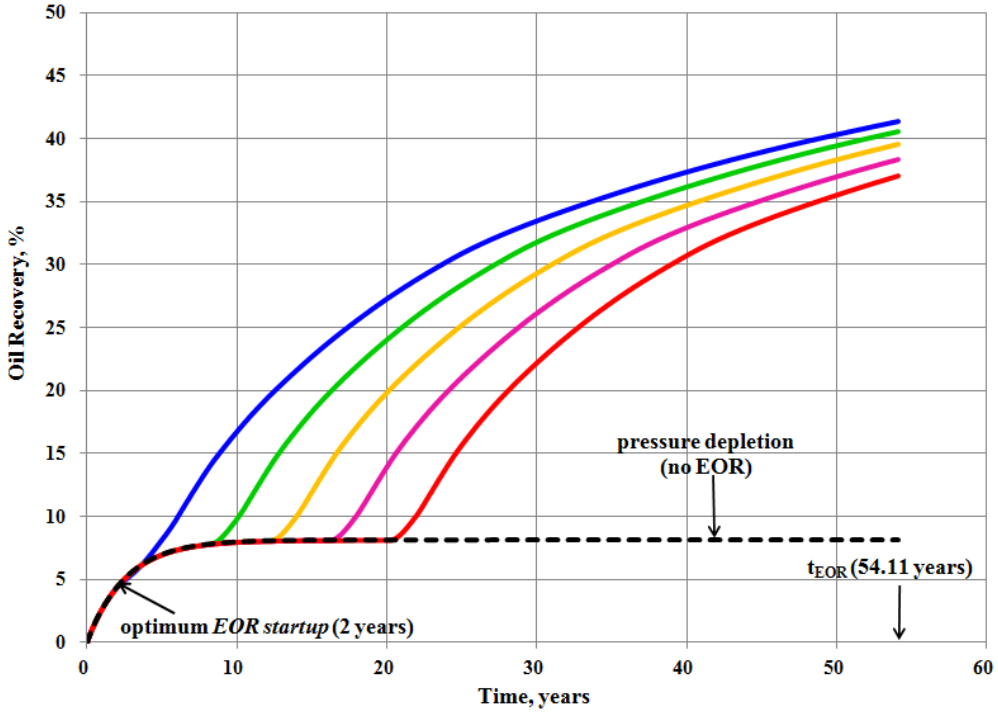

Figure 28- Comparison between recoveries from optimum t_D and those from other t_D's over t_{EOR} for a 4-spot well pattern

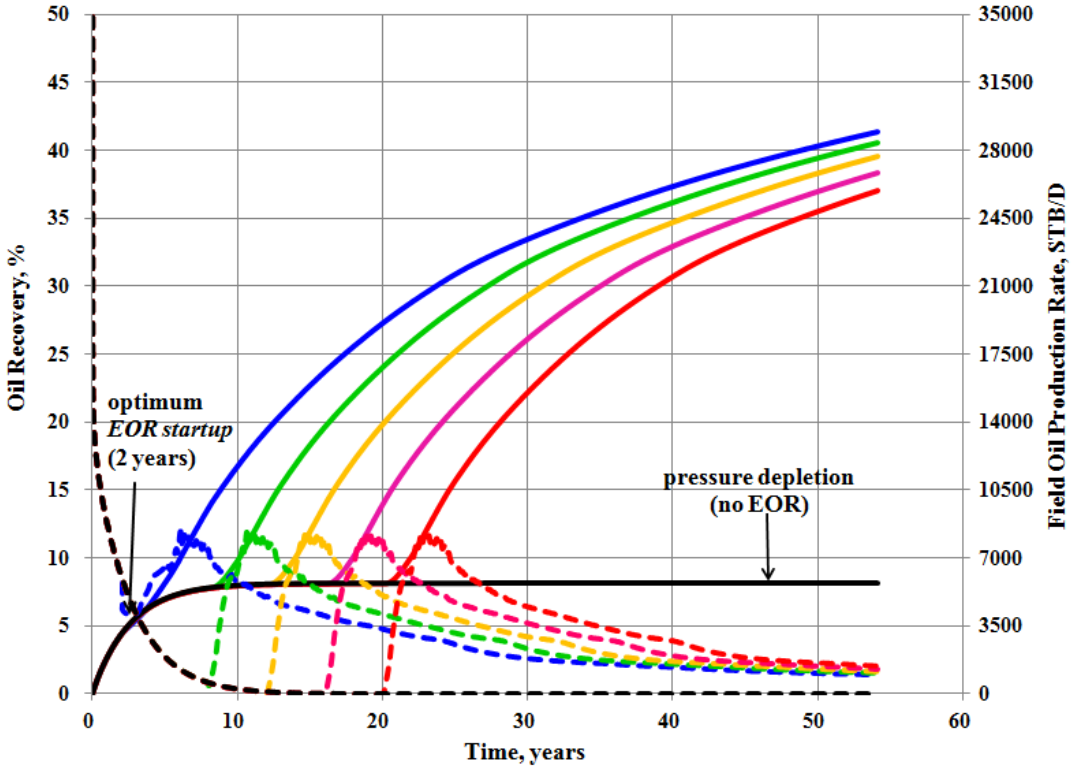

Figure 29-Effect of EOR startup time on oil production rate and oil recovery

Unlike the case of optimum 2-spot and 3-spot well patterns, for the case of optimum 4-spot well pattern, we observed non-uniform pressure distribution in the grid blocks of all the 3

layers in the model regardless of their permeability. This is shown for the 3 grid blocks of layer 1 in **Figs. 30, 31, and 32.** The non-uniform pressure distribution in all layers resulted in a pressure range of about 12700 to 13800 psia in the model. However, this pressure range was below the injection pressure of 15000 psia in the model and, hence, no problem in wellbore injectivity was observed at t_D.

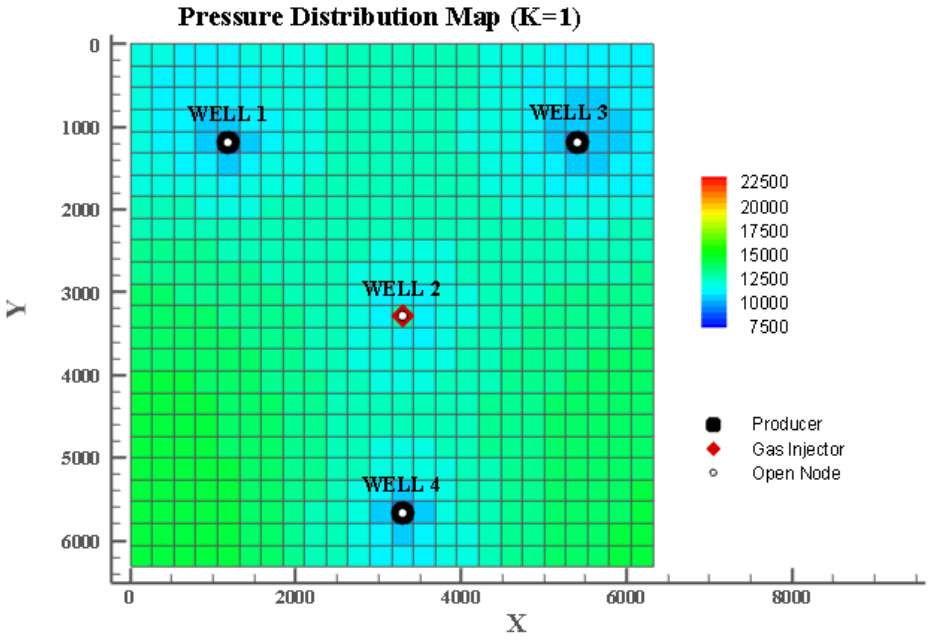

Figure 30- Non-uniform pressure distribution in grid block 1 of layer 1with k=30 md at optimum t_D and for optimum well spacing

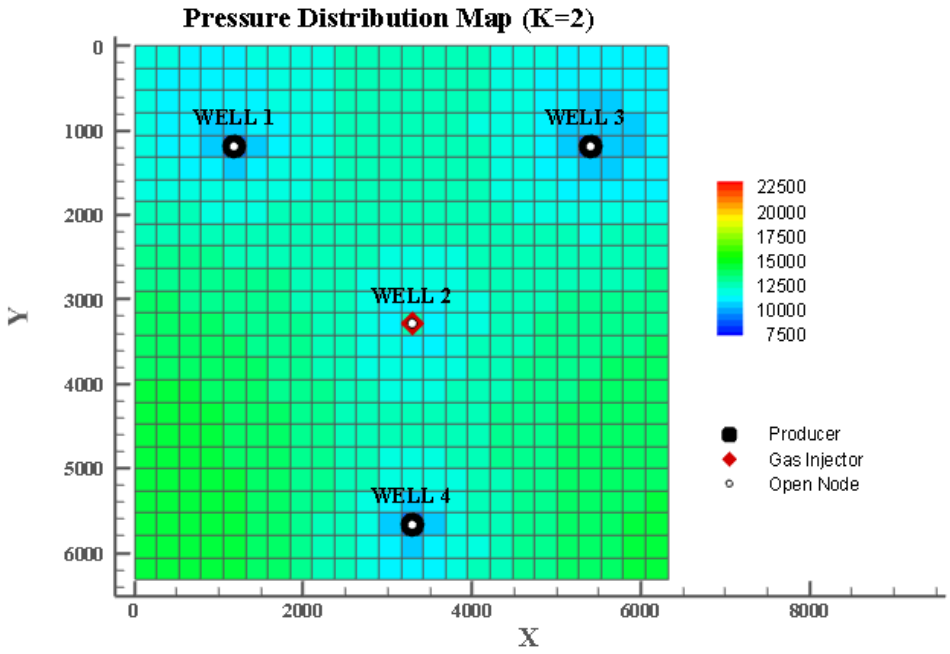

Figure 31- Non-uniform pressure distribution in grid block 2 of layer 1with k=19 md at optimum t_D a d for optimum well spacing

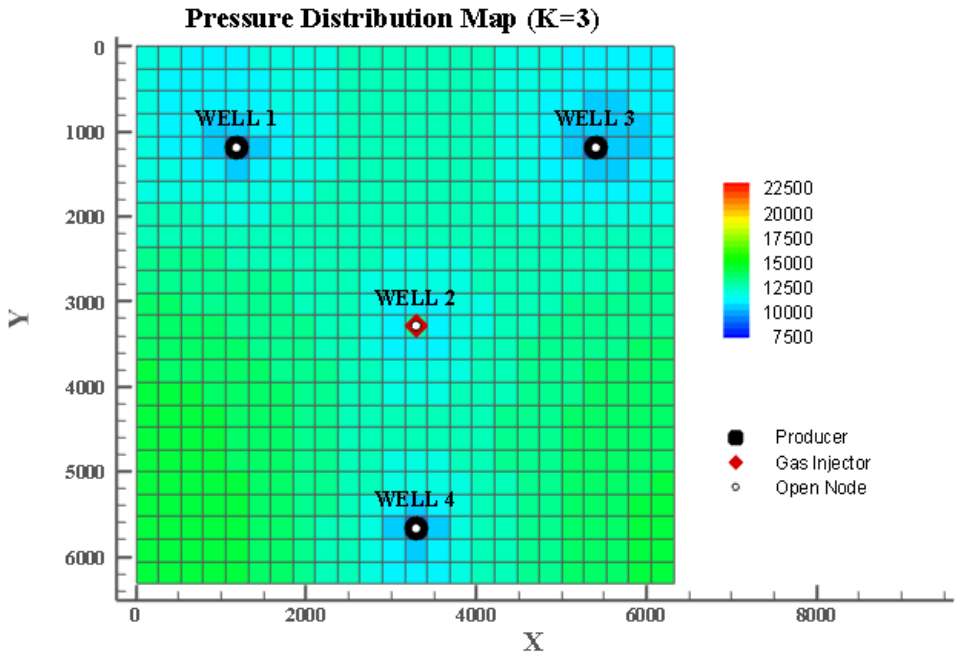

Figure 32- Non-uniform pressure distribution in grid block 3 of layer 1 with k=0.3 md at optimum t_D and for optimum well spacing

4.5 Well Spacing and t_D Optimization for 5-Spot Well Pattern

In the 5-spot well pattern, 4 wells (wells 1, 3, 4, and 5) were located on the 4 vertices of a square and the 5th well (well 2) was placed at the center of the square. Well 2 was permanently positioned at the center of the square while the other 4 well on the vertices of the square were moved uniformly away from well 2 through the optimization process to find the optimum well spacing for the 5-spot well pattern. Sensitivity to t_D was also done for each 5-spot well pattern to find the optimum t_D.

To reduce the number of simulation runs, a sensitivity analysis was done similar to those done for the other well patterns studied earlier. The analysis was done to investigate the effect of moving the wells in the model to the boundaries and corners of the model on cumulative oil production. The sensitivity was done for all possible 5-spot well patterns along AA′, BB′, CC′, and DD′ lines shown in **Fig. 33.** Well 2 at the center of the 5-spot well patterns was moved along these lines and cumulative oil production for 20 years of pressure depletion for all the possible 5-spot patterns along these lines were compared **(Fig. 34).**

The sensitivity analysis showed that as wells in the 5-spot well pattern get closer to the boundaries and corners of the model, cumulative production decreases. Similar results to the ones shown in Fig. 34 were observed for the case of pressure depletion followed by miscible CO_2 flooding. Based on this conclusion, the optimization process was done only along AA′, BB′, and CC′ lines.

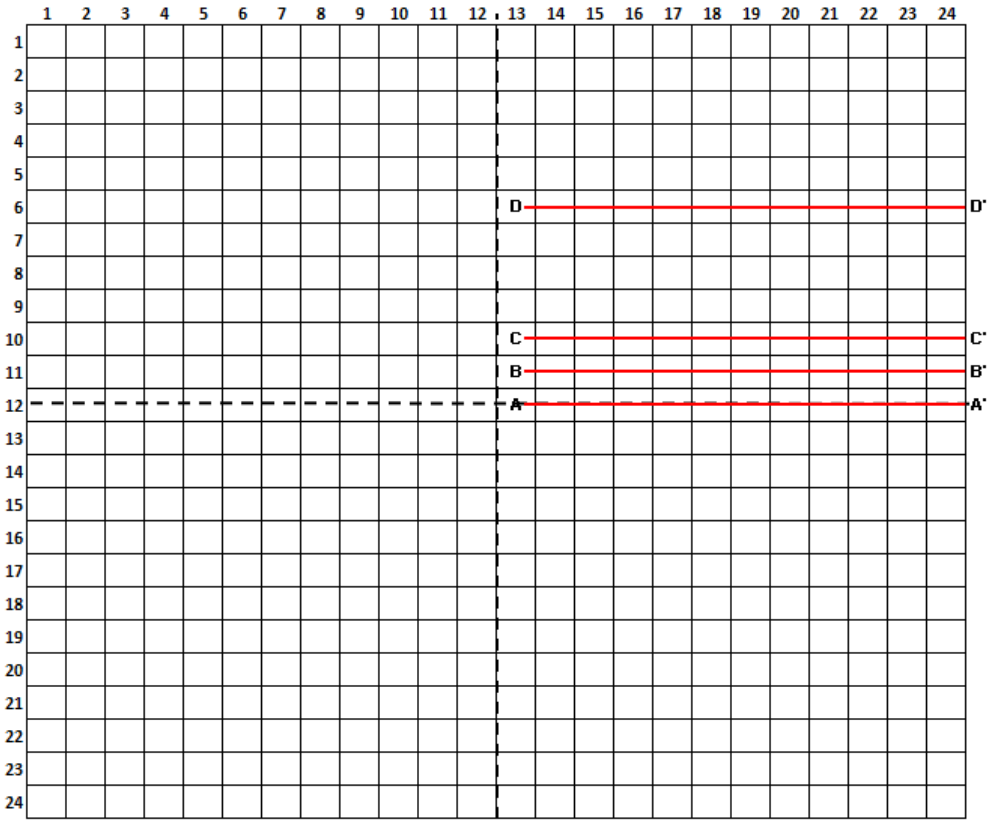

Figure 33- Moving well positions to the boundaries and corners of the model

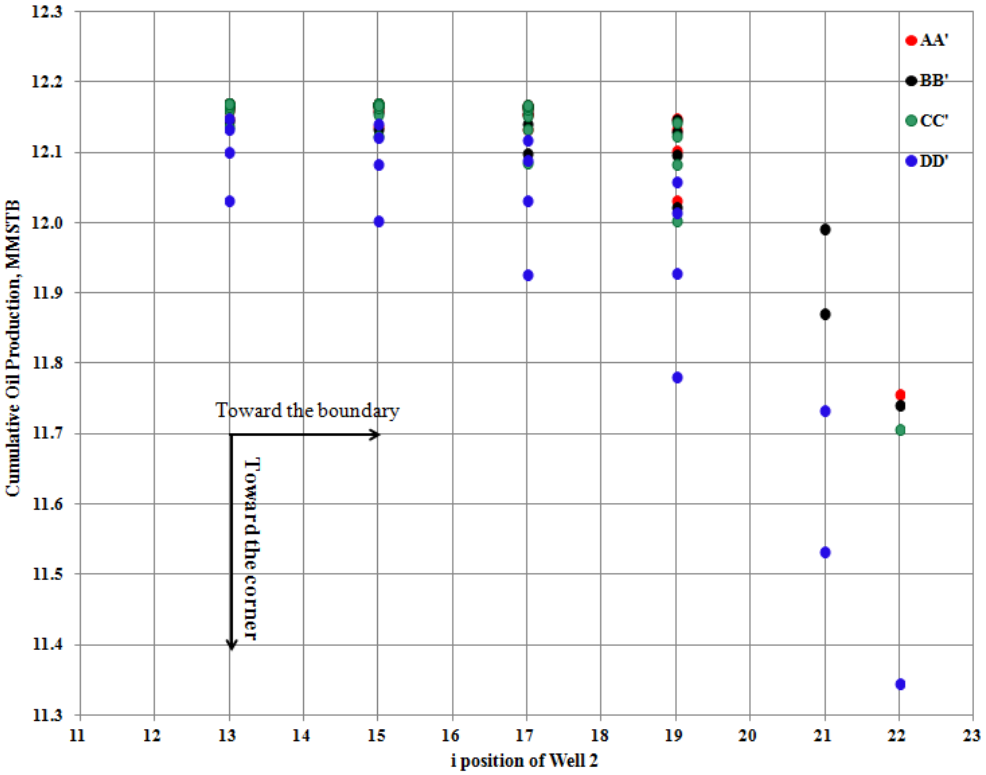

Figure 34- Cumulative oil production after 20 years of pressure depletion for different 5-spot well spacings along AA', BB', CC', and DD' lines

Table 15 gives the optimum well spacing and t_D found in optimization of the 5-spot well pattern consisting of 341 simulation runs. These optimum parameters gave maximum cumulative oil production of 65.963 MMSTB over t_{EOR} of 48.76 years which is equivalent to an oil recovery of 43.96%.

Table 15-Optimum well locations and EOR startup time for 5-spot well pattern

Optimum Well Locations (I,J)					Optimum t_D, years
Well 1	Well 2	Well 3	Well 4	Well 5	1.64
(5,4)	(13,12)	(21,4)	(21,20)	(5,20)	

Figure 35 compares the oil recovery from the optimum t_D (1.64 years) and well spacing with those from the same well spacing but later CO_2 injection startup times.

Similar to other well patterns studied earlier, as shown in **Fig. 36,** for the 5-spot well pattern, higher oil production rate is maintained for a longer time in the case of the optimum t_D which in consequence results in maximized cumulative oil production over t_{EOR}.

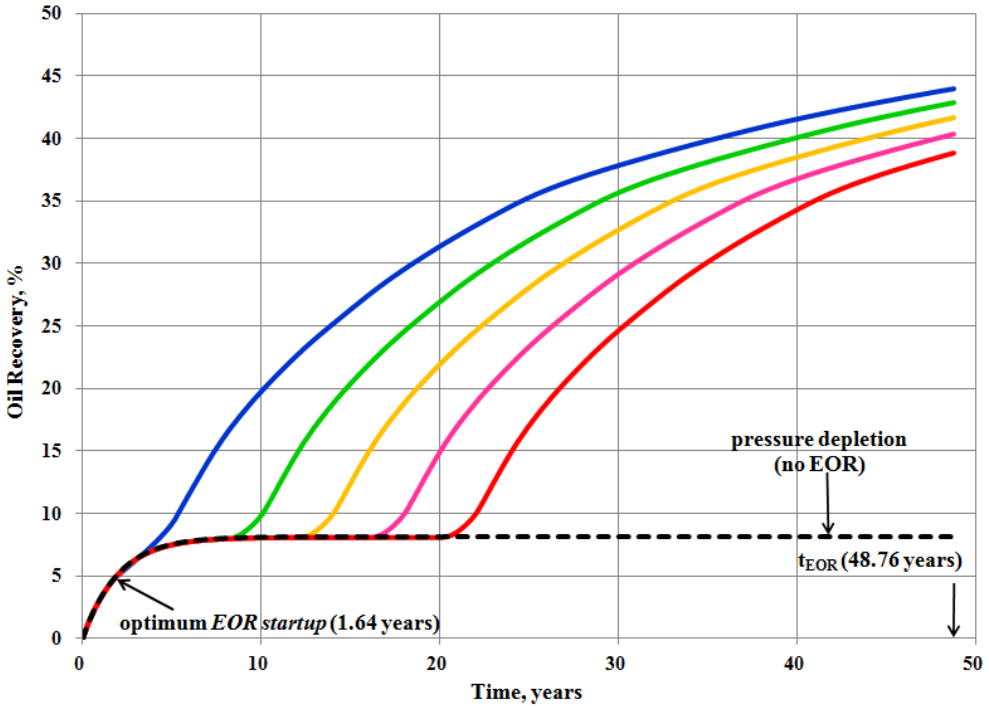

Figure 35- Comparison between recoveries from optimum t_D and those from other t_D's over t_{EOR} for a 5-spot well pattern

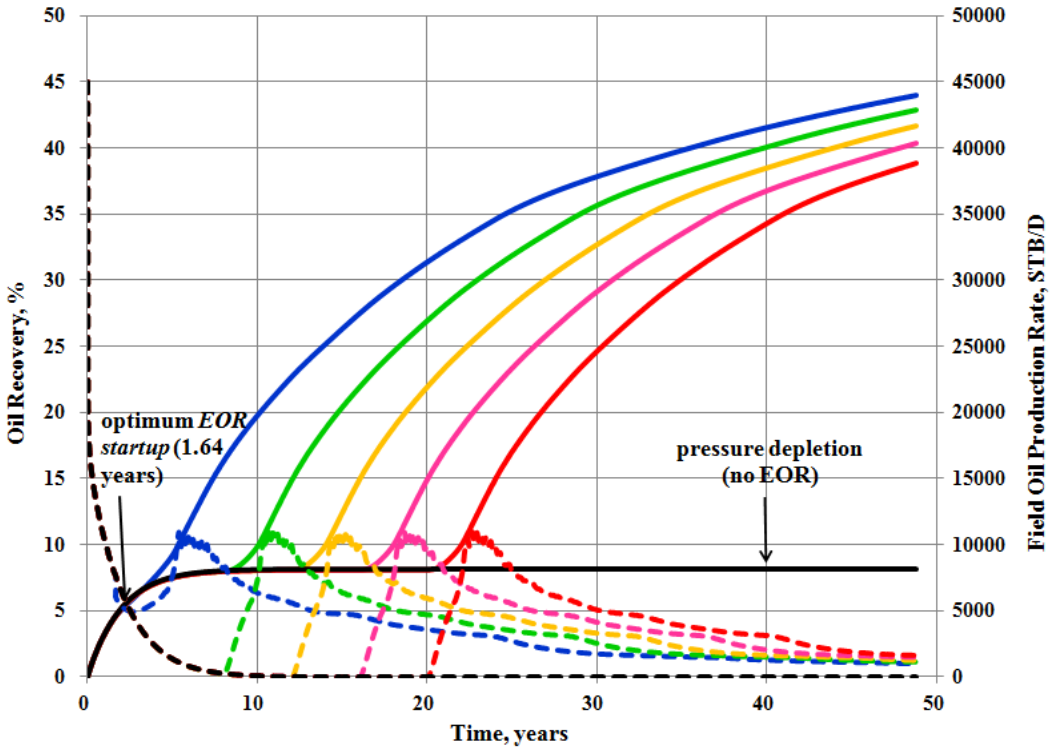

Figure 36- Effect of EOR startup time on oil production rate and oil recovery

Like the case of optimum 4-spot well pattern, for the 5-spot well pattern, we observed non-uniform pressure distribution in the grid blocks of all the 3 layers in the model regardless of their permeability. This is shown for the 3 grid blocks of layer 1 in **Figs. 37, 38, and 39.** The non-uniform pressure distribution shows a pressure range of 10900 to 12900 psia in the model. However, this pressure range is below the injection pressure of 15000 psia in the model and, hence, no problem in wellbore injectivity was observed at t_D.

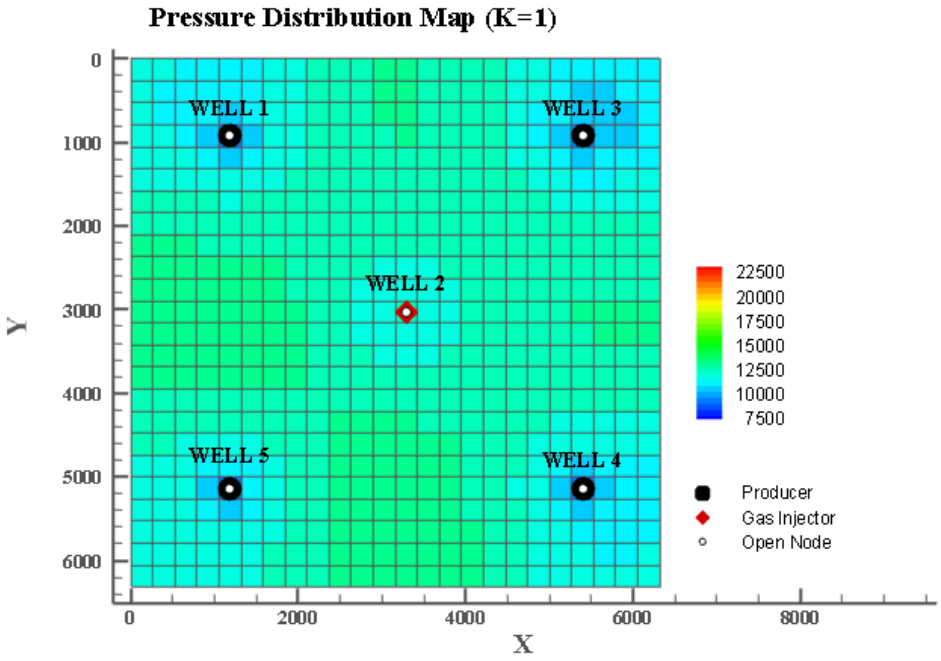

Figure 37-Non-uniform pressure distribution in grid block 1 of layer 1with k=30 md at optimum t_D and for optimum well spacing

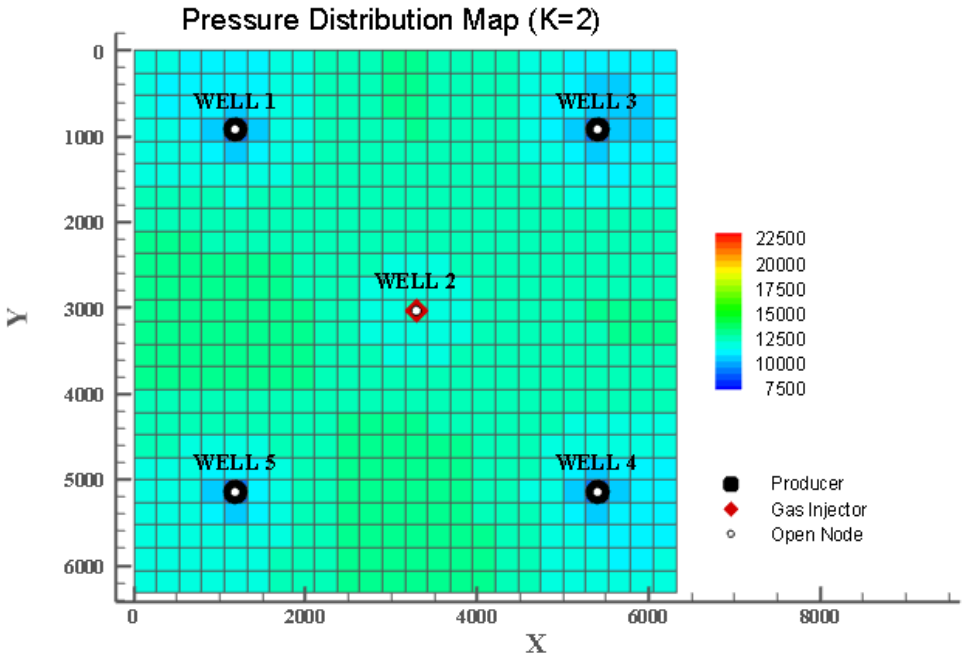

Figure 38-Non-uniform pressure distribution in grid block 2 of layer 1 with k=19 md at optimum t_D and for optimum well spacing

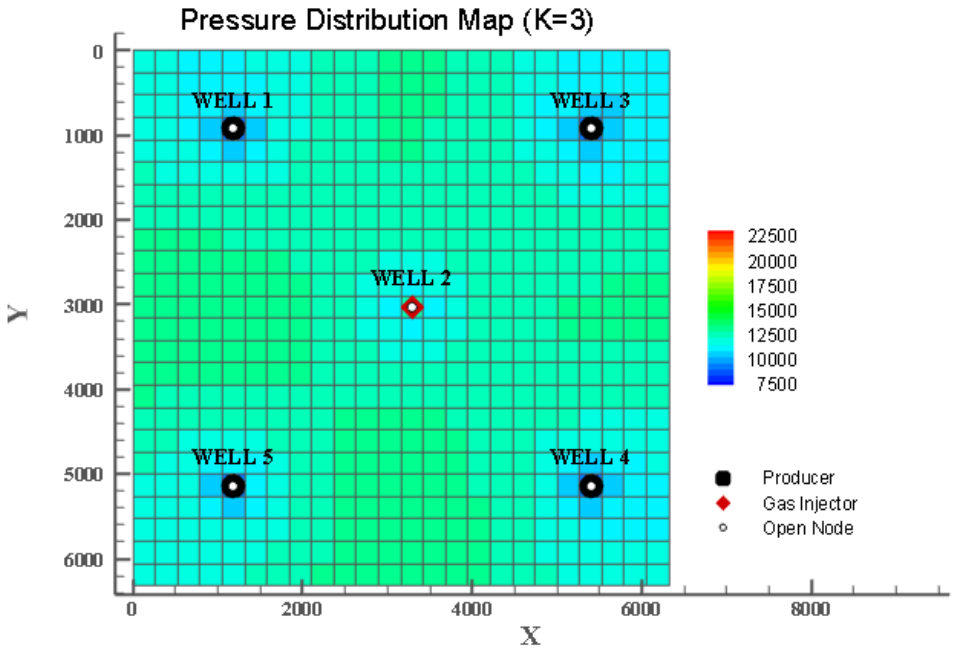

Figure 39-Non-uniform pressure distribution in grid block 3 of layer 1 with k=0.3 md at optimum t_D and for optimum well spacing

4.6 Effect of Optimized Well Pattern on Cumulative Oil Production and Incremental Oil Recovery

In Sections 4.2 to 4.5, the effect of optimized well spacing and t_D for different well patterns was discussed. However, no comparison was done for the effect of optimized well patterns on the cumulative oil production and incremental oil recovery.

Table 16 gives a comparison between the optimization results of different well patterns studied earlier.

Table 16-Comparison of the optimization results for different well patterns

Well Pattern	t_{EOR}, years	Optimum t_D, years	Maximum Cumulative Oil Production, MMSTB	Maximum Oil Recovery, %
2-spot	63.84	5.20	44.876	29.90
3-spot	59.31	3.15	57.443	38.29
4-spot	54.11	2.00	62.245	41.36
5-spot	48.76	1.64	65.963	43.96

Figures 40 to 42 compare the effect of each of the discussed optimized well patterns in terms of well spacing and t_D on cumulative oil production and incremental oil recovery for pressure depletion of the reservoir followed by miscible CO_2 injection.

According to Figs. 40 to 42, both cumulative oil production and incremental oil recovery increased with increasing the number of wells in an optimum way.

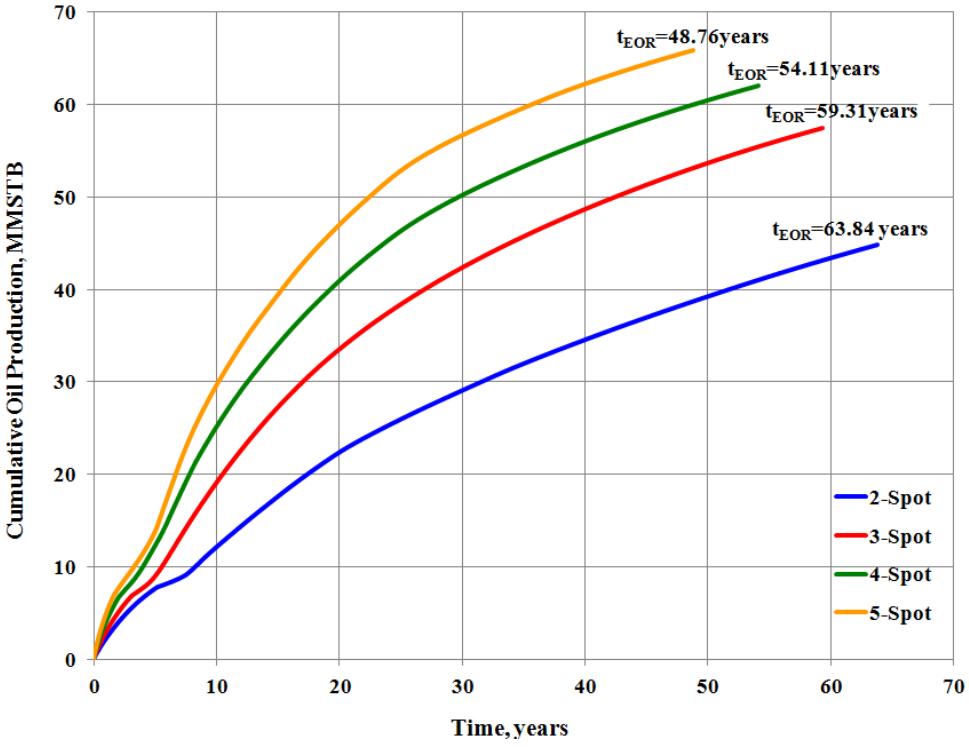

Figure 40- Effect of optimized well pattern on cumulative oil production

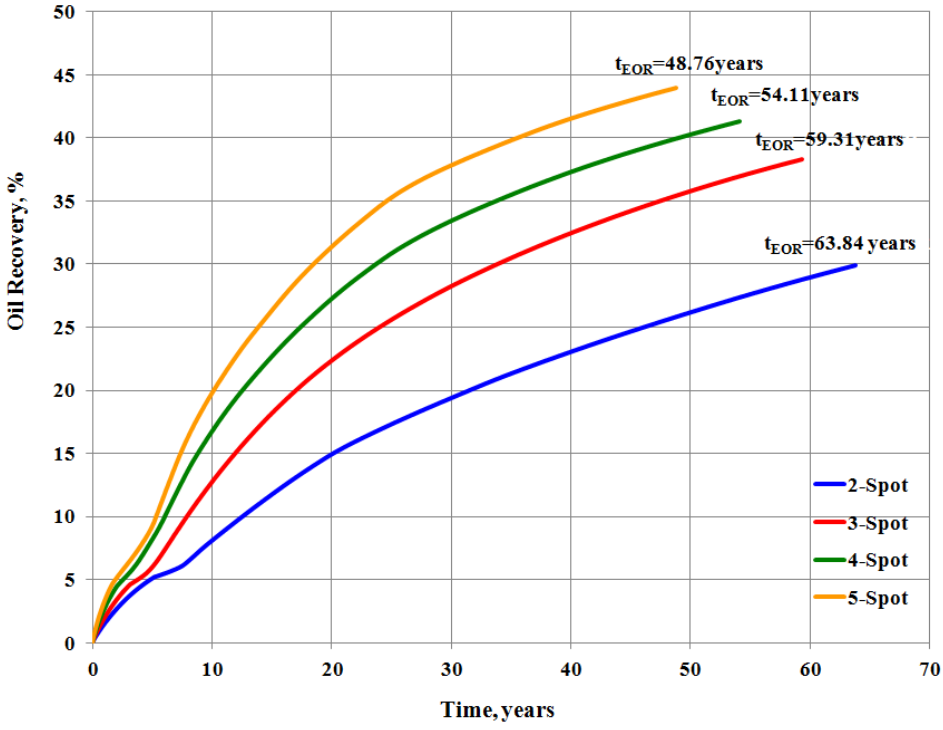

Figure 41-Effect of optimized well pattern on oil recovery

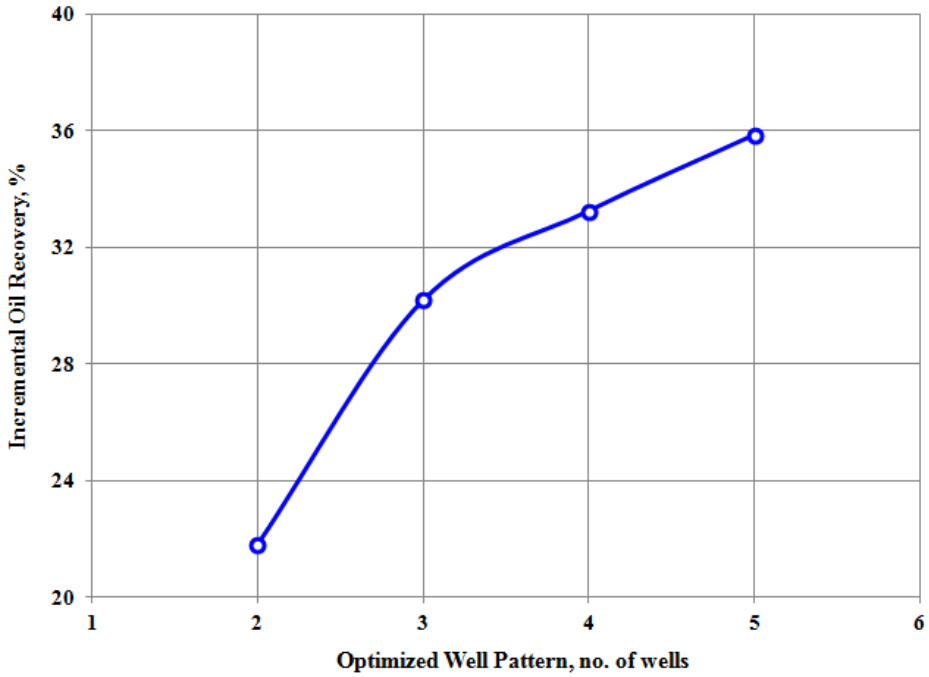

Figure 42-Effect of optimized well pattern (number of wells) on incremental oil recovery

Chapter 5: Conclusions

A compositional model was made up in this study with the help of limited data available for Wilcox formation in the Gulf of Mexico to represent an ultradeep, high pressure reservoir. The model was then used to investigate the effect of number of wells, EOR startup time, well spacing, and well placement on the incremental and cumulative oil recovery of depletion of the reservoir followed by miscible CO_2 injection. Hundreds and sometimes thousands of simulation runs were done to find the optimum well spacing and CO_2 injection startup time for each well pattern representing a specified well placement and number of wells. On the basis of the results and discussions made in Chapter 4, the following conclusions can be drawn:

1. Miscible CO_2 injection strategy could result in considerable incremental oil recovery in the ultradeep, high pressure reservoir under study.

2. Both incremental oil recovery and cumulative oil recovery were increased with number of wells on the model.

3. No pressure isolation region was left after primary depletion of the reservoir in any of the well pattern scenarios and, hence, no problem with injectivity was observed in all scenarios. This was most probably due to the fact that the reservoir was neither stratigraphically nor structurally compartmentalized in the model.

4. The higher the number of wells, the earlier the optimized startup time. Therefore, the optimized EOR startup time is dependent on the well pattern.

5. Sensitivity analysis for well positions with respect to the boundaries and corners of the model was done before optimization process and it considerably reduced the number of simulation runs in the optimization process.

6. The optimum location on the model for the injector (well 2) at the center of the 4-spot and 5-spot well patterns is the center of the model.

Chapter 6: Recommendations for Future Research

The following recommendations can be made based on the results discussed in Chapter 4 and conclusions made in the previous chapter. Some of these recommendations can be used to conduct further research in the field of ultradeep, high pressure reservoirs.

1. Although miscible CO_2 flooding resulted in considerable incremental oil recovery, this EOR strategy should be evaluated economically and its feasibility should be studied in terms of CO_2 availability.

2. The optimization process in this study did not consider any economic evaluation. In other terms, the optimization process was conducted only from physical ultimate recovery perspective. Optimization can also be done to maximize economic ultimate recovery to take into account the economic aspects of field development.

3. Other EOR strategy such as water flooding and miscible natural gas injection should be studied and the results should be compared with those of miscible CO_2 flooding.

4. We did not consider any aquifer in the model. The effect of an aquifer on the optimized variables can be studied.

5. No reservoir compartmentalization was considered in the model. To see the effect of reservoir compartmentalization on pressure distribution just before EOR startup, the model should be compartmentalized structurally or stratigraphically.

References

1. Beal, C. 1946. The Viscosity of Air, Water, Natural Gas, Crude Oil and Its Associated Gases at Oil Field Temperatures and Pressures. *In Trans. of the AIME,* Vol. 165, Issue. 1, 95-115: The American Institute of Mining, Metallurgical, and Petroleum Engineers Inc. ISSN 0081-1696.
2. Chew, J.N. and Connally, C.A. 1959. A Viscosity Correlation for Gas-Saturated Crude Oils. *In Trans. of the AIME,* Vol. 216, 23-25: The American Institute of Mining, Metallurgical, and Petroleum Engineers Inc.
3. Dranchuk, P.M. and Abou-Kassem, H. 1975. Calculation of Z Factors for Natural Gases Using Equations of State. *J. Cdn. Pet. Tech*. 14 (3): 34. PETSOC-75-03-03. http://dx.doi.org/10.2118/75-03-03.
4. Dusterhoft, R., Strobel, M., and Szatny, M. 2012. An Automated Software Workflow To Optimize Gulf of Mexico Lower Tertiary Wilcox Sand Reservoirs. Paper SPE 151754 presented at the SPE International Symposium and Exhibition on Formation Damage Control, Lafayette, Louisiana, USA, 15-17 February. http://dx.doi.org/10.2118/151754-MS.
5. Haajizadeh, M., Fayers, F.J., Cockin, A.P. et al. 1999. On the importance of Dispersion and Heterogeneity in the Compositional Simulation of Miscible Gas Processes. Paper SPE 57264 presented at the SPE Asia Pacific Improved Oil Recovery Conference, Kuala Lumpur, Malaysia, 25-26 October. http://dx.doi.org/10.2118/57264-MS.
6. Haajizadeh, M., Fayers, F.J., Cockin, A.P. 2000. Effects of Phase Behavior, Dispersion and Gridding on Sweep Patterns for Nearly Miscible Gas Displacement. Paper SPE 62995 presented at the SPE Annual Technical Conference and Exhibition, Dallas, Texas, 1-4 October. http://dx.doi.org/10.2118/62995-MS.
7. Johns, R.T., Fayers, F.J., and Orr, F. 1992. Effect of Gas Enrichment and Dispersion on Nearly Miscible Displacements in Condensing/Vaporizing Drives. Paper SPE 24938 presented at the 67th SPE Annual Technical Conference and Exhibition, Washington, DC, 4-7 October. http://dx.doi.org/10.2118/24938-PA.
8. Khatib, A.K., Earlougher, R.C., and Kantar, K. 1981. CO2 Injection as an Immiscible Application for Enhanced Recovery in Heavy Oil Reservoirs. Paper SPE 9928 presented at the SPE California Regional Meeting, Bakersfield, California, 25-27 March. http://dx.doi.org/10.2118/9928-MS.
9. Killough, J.E. and Kossack, C.A. 1987. Fifth Comparative Solution Project: Evaluation of Miscible Flood Simulators. Paper SPE 16000 presented at the Ninth SPE Symposium on Reservoir Simulation, San Antonio, Texas, 1-4 February. http://dx.doi.org/10.2118/16000-MS.

10. Lee, A.L., Gonzalez, M.H., and Eakin, B.E. 1966. The viscosity of Natural Gases. *In Transactions of Society of Petroleum Engineers*, Vol. 18, Issue 08, 997-1,000. Society of Petroleum Engineers. ISSN 0149-2136. http://dx.doi.org/10.2118/1340-PA.

11. Lewis, J., Clinch, S., Mayer, D. et al. 2007. Exploration and Appraisal Challenges in the Gulf of Mexico Deep-Water Wilcox: Part 1-Exploration Overview, Reservoir Quality, and Seismic Imaging. Presented at the 27th Annual Gulf Coast Section SEPM Foundation Bob F. Perkins Research Conference, Huston, Texas, USA, 2-5 December.

12. McCain, W.D. Jr. 1991. Reservoir-Fluid Property Correlations-State of the Art. *SPE Res Eng* **6**(2): 266-272. SPE-18571. http://dx.doi.org/10.2118/18571-PA.

13. Lim, M.T., Pope, G.A., Sepehrnoori, K., et al. 1997. Grid Refinement Study of a Hydrocarbon Miscible Gas Injection Reservoir. Paper SPE 38060 presented at the SPE Asia Pacific Oil and Gas Conference, Kuala Lumpur, Malaysia, 14-16 April. http://dx.doi.org/10.2118/38060-MS.

14. Muskat, M. 1949. Physical Principles of Oil Production, first edition, New York: McGraw-Hill Book Company.

15. Oilfield Glossary. 2014. First-Contact Miscibility http://www.glossary.oilfield.slb.com/en/Terms/f/first-contact_miscibility.aspx (accessed 24 May 2014).

16. Oilfield Glossary. 2014. Multiple-Contact Miscibility http://www.glossary.oilfield.slb.com/en/Terms/m/multiple-contact_miscibility.aspx (accessed 22 May 2014).

17. Peaceman, D.W. 1983. Interpretation of Well-Block Pressures in Numerical Reservoir Simulation With Nonsquare Grid Blocks and Anisotropic Permeability. *SPE J.* **23**(3): 531-543. SPE-10528-PA. http://dx.doi.org/10.2118/10528-PA.

18. Petrosky, G.E. and Farshad, F.F. 1993. Pressure-Volume-Temperature Correlations for Gulf of Mexico Crude Oils. Paper SPE 26644 presented at the SPE Annual Technical Conference and Exhibition, Houston, Texas, 3-6 October. http://dx.doi.org/10.2118/26644-MS.

19. Petrowiki. 2013. Designing a Miscible Flood (19 August 2013 revision) http://petrowiki.org/Designing_a_miscible_flood (accessed 25 May 2014).

20. Petrowiki. 2013. Miscible Flooding (19 August 2013 revision) http://petrowiki.org/Miscible_flooding (accessed 25 May 2014).

21. Rains, D.B., Zarra, L., and Meyer, D. 2007. The Lower Tertiary Wilcox Trend in the Deep Water Gulf of Mexico. Presented at the AAPG Annual Convention, Long Beach California, USA, 1-3 April.

22. Solano, R., Lee, S.T., Ballin, P.R. et al. 2001. Evaluation of the Effects of Heterogeneity, Grid Refinement, and Capillary Pressure on Recovery for Miscible-Gas Injection Processes. Paper SPE 71602 presented at the SPE Annual Technical

Conference and Exhibition, New Orleans, Louisiana, , 30 September-3 October. http://dx.doi.org/10.2118/71602-MS.

23. Stalkup, F.L. 1990. Effect of Gas enrichment and Numerical Dispersion on Enriched-Gas-Drive Predictions. *SPE Res Eng* **5**(4): 647-655. http://dx.doi.org/10.2118/18060-PA.

24. Sutton, R.P. 1985. Compressibility Factors for High-Molecular-Weight Reservoir Gases. Paper SPE 14265 presented at the SPE Annual Technical Conference and Exhibition, Las Vegas, Nevada, 22-26 September. http://dx.doi.org/10.2118/14265-MS.

25. Standing, M.B. 1981. *Volumetric and Phase Behavior of Oil Field Hydrocarbon Systems*, Richardson, Texas: Textbook Series, SPE.

26. Whitson, H.C. and Brule´, M.R. 2000. *Phase Behavior*, Vol. 20, 18-46, Richardson, Texas: Monograph Series, SPE.

27. SENSOR Manual, 2011: Coats Engineering, Inc.

28. Vasquez, M.E. and Beggs, H.D. 1980. Correlations for Fluid Physical Property Prediction. *J. Pet. Tech* **32**(6): 968-970. SPE-6719. http://dx.doi.org/10.2118/6719-PA.

Appendix 1 - SENSOR Data File Structure

```
C                    **START OF INITIAL DATA**
TITLE
   . . . any number of 132-column alphanumeric lines. . .
ENDTITLE
GRID Nx Ny Nz
C                          default solver is RBILU(0)
C                          default formulation is IMPES
D4                         ! if the direct-solution D4 solver is to be used
NF                         ! if the Nested Factorization solver is to be used
IMPLICIT                   ! if the fully implicit formulation is to be used
MISC . . . 6 numbers . . .  ! water properties, pref
PVTEOS                     ! if this is a compositional problem
  . . . EOS data . . .
PVTBO                      ! if this is a back oil problem
   . . . black oil PVT table . . .
SWT   n   (SGT   n)
   . . . tables giving kr and pc vs. saturation . . .
COMPACTABLE                ! if compaction is used for rock compressibility
   . . . compaction tables . . .
DEPTH     VALUE or  CON or ZVAR or . . . etc.
   . . . array data . . .
THICKNESS   VALUE or . . .
   . . . array data . . .
KX   (and/or TX)    VALUE or . . .
   . . . array data . . .
KY   (and/or TY)    VALUE or . . .
   . . . array data . . .
KY   (and/or TY)    VALUE or . . .
   . . . array data . . .
POROS   (and/or PV)     VALUE or . . .
   . . . array data . . .
SEP                        ! surface separator data if a compositional problem
   . . . data . . .
INITIAL
   . . . data specifying initial P, WOC, GOC, etc. . . .
ENDINIT                    ! end of Initial Data
C                          **MODIFICATION DATA START HERE**
MODIFY  PV                 ! optional,  to modify pore volumes
   . . . data . . .
MODIFY  TX                 ! optional,  to modify transmissibility Tx
  . . . data . . .
  . . . other optional additional MODIFY data . . .
C                          **RECURRENT DATA START HERE**
C                          WELL data must precede other well data
WELL
  . . . well locations and perforations data . . .
```

```
C                              Remaining data here are order independent
C                              Except for chronological order of TIME  and data changes
WELLTYPE
   . . . defines wells as producers or injectors, and defines units . . .
LIMITWELL                      ! optional
   . . . economic limit data for wells . . .
BHP                            ! for wells not using Tubing Head Pressure (THP) tables
   . . . minimum flowing Bottomhole Pressure (BHP) wells . . .
THP                            ! for wells using THP tables
   . . . minimum wellhead pressures for THP wells . . .
THPTABLE                       ! needed only if there are THP wells
  . . . tubinghead pressure tables for THP wells . . .
RATE
  . . . well rate data . . .
WELLPLAT                       ! if any platforms are to be used
  . . . assign wells to platforms . . .
  . . . other platform keywords/data . . .
LIMITFIELD   . . . 5 numbers . . .     ! optional field economic limit data
TIME  t1                       ! proceed to time = t1
TIME  t1  dtime                ! optional, in place of previous line,
C                              proceed to time t1, with printout every dtime days
WELL                           ! optional, to add new wells or change perforations of old ones
  . . . data . . .
RATE                           ! optional, to change well rates (default rates are shut in, with no  recirculation
  . . . data . . .
TIME  t2                       ! proceed to time = t2
  . . . WELL, RATE, etc. data changes . . .
TIME t3
   . . . etc . . . data changes . . . time entries . . .
  . . .
TIME tlast
END                            **END OF DATA FILE**
```

Appendix 2 – From Compositional to Black Oil

```
TITLE
 Compositional to Black Oil
ENDTITLE
GRID   24  24   10
CPU
MISC   1.0  3.0E-6  62.4   0.7   1.0E-6   5000
KRANALYTICAL
  0.2   0.2   0.0   0.0
  1.0   1.0   1.0   1.0
  2.0   2.0   2.0   2.0
DELX CON
  24*267.38
DELY CON
  24*267.38
THICKNESS  ZVAR
  3*6.82 4*7.535 3*29.8
POROS CON
  0.2
DEPTH CON
  24606
KX  ZVAR
  3*20.40  4*6.12  3*1.10
KY  EQUALS  KX
KZ  EQUALS  KX
MOD
  1 24 1 24 1 10 * 0.1
 BLACKOIL    1   15   31   EXTEND
PRESSURES   14.7  250   500  750  1000  1160.30  1500  2000  2250  2500  2750  2800  3000  4000  5000  6000
7000  8000  9000  10000  11000  12000  13000  14000  15000  16000  17000  18000  19000  20000  20300
RESERVOIR FLUID
   0.000000   0.000000   0.280743    0.043155    0.100696    0.287703   0.215777    0.071926
INJECTION GAS
  1  0  0  0  0  0  0  0
ENDBLACKOIL
PVTEOS
  200
  CPT        PC          TC           MW          AC       ZCRIT      SHIFT      OMEGA     OMEGB       PCHOR
  CO2   1069.51       547.42       44.010     0.2250   0.27433    0.00189    0.45724     0.0778         80.0
  N2     491.680      227.29       28.000     0.0400   0.29178   -0.16453    0.45724     0.0778         59.1
  C1     667.800      343.00       16.040     0.0130   0.29345   -0.15193    0.45724     0.0778         71.0
  C3     616.300      665.70       44.100     0.1524   0.27630    -0.06428   0.45724     0 .0778        151.0
  C6     436.900      913.40       86.180     0.3007   0.25862    0.09681    0.45724     0.0778         241.8
  C10    304.000     1111.80      142.290     0.4885   0.23435    0.20911    0.45724     0.0788         376.5
  C15    200.000     1270.00      206.000     0.6500   0.19872    0.40916    0.45724     0.0778         529.4
     C20   162.0000 1380.0000  282.0000  .8500000  0.20143    0.40155  .4572400   .0788       711.80
BIN
```

```
-0.02000  0.10000  0.13500  0.10000  0.10000  0.10000  0.10000
          0.03600  0.08000  0.10020  0.10000  0.10000  0.10000
                   0.00000  0.00000  0.00000  0.05000  0.05000
                            0.00000  0.00000  0.00500  0.00500
                                     0.00000  0.00000  0.00000
                                              0.00000  0.00000
                                                       0.00000
PSM
INITIAL
DEPTH     PSATBP
 24606     1160.3
PINIT   20300
ZINIT   24606
ENDINIT
WELL
  I       J     K     PI
WELL1
 17     8     1    0.413
 17     8     2    0.413
 17     8     3    0.413
 17     8     4    0.137
 17     8     5    0.137
 17     8     6    0.137
 17     8     7    0.137
 17     8     8    0.097
 17     8     9    0.097
 17     8    10    0.097
WELL2
 8      17     1    0.413
 8      17     2    0.413
 8      17     3    0.413
 8      17     4    0.137
 8      17     5    0.137
 8      17     6    0.137
 8      17     7    0.137
 8      17     8    0.097
 8      17     9    0.097
 8      17    10    0.097

WELLTYPE
WELL1   STBOIL
WELL2   MCFINJ
INJGAS
WELL2
 1  0  0  0  0  0  0  0
BHP
WELL1    5000
WELL2  15000
```

```
RATE
WELL1  1.E10
WELL2  1.E10
TIME 7300 100
END
```

Appendix 3 – PhazeComp Data File for MMP Estimation

```
TITLE "MMP Calculations"

TEST1 ON
TEST2 ON

CHAR
EOS PR
Component    MW       Tc(R)      Pc(psia)    AF
CO2          44.01    547.420    1069.51     0.2250
N2           28.00    227.290    491.68      0.0400
C1           16.040   343.000    667.80      0.0130
C3           44.100   665.700    616.30      0.1524
C6           86.180   913.400    436.90      0.3007
C10          142.29   1111.80    304.00      0.4885
C15          206.00   1270.00    200.00      0.6500
C20          282.00   1380.00    162.00      0.8500

Binaries  CO2   N2      C1      C3      C6      C10     C15     C20
CO2           -0.02   0.10    0.135   0.1     0.1     0.1     0.1
N2                    0.036   0.08    0.1002  0.1     0.1     0.1
C1                            0       0       0       0.05    0.05
C3                                    0       0       0.005   0.005
C6                                            0       0       0
C10                                                   0       0
C15                                                   0       0
C20
END

MIX OIL  0.0  0.0  0.280743  0.043155  0.100696  0.287703  0.215777  0.071926
MIX INJE  1    0     0     0     0     0     0     0
MIX FEED OIL 1 MOLE
TEMP 200 F
PRESS 0 PSIA
MIX FEED OIL 1 MOLE
TEMP 200 F
PRES PSIA
PSAT
MMP STAGES 500
EOF
```

Appendix 4 – Submitted Paper Based on the Thesis Work

A paper was submitted to the 19th Middles East Oil & Gas Show Conference and is still pending for approval by the review committee. The same paper will be submitted to similar EAGE and SPE events.

Control/Tracking Number: 15MEOS-P-1431-SPE
Activity: Proposal
Current Date/Time: 5/25/2014 7:03:56 AM

Effect of Well Spacing and Well Placement Optimization On Ultimate and Incremental Oil Recoveries In An Ultradeep, High Pressure Oil Reservoir: A Simulation Study

Author Block: A. Hossein Zadeh, Norwegian University of Science and Technology; J. Kleppe, Norwegian University of Science & Tech; M. Ghasemi, C. Whitson, Norwegian University of Science and Technology

Abstract:
Exploitation of ultradeep, high pressure oil reservoirs is always associated with numerous risks and challenges. One of the most pronounced constraints in development of such fields is the number of wells, which is imposed by massively high cost of drilling. Low number of wells may lead to high pressure isolation regions left after primary production of the reservoir. Ultradeep reservoirs with high pressure are more prone to such leftover high pressure isolation regions due to their low permeable characteristic. These regions can, subsequently, deteriorate the efficiency of EOR as the injected fluid cannot access the residual oil in these regions. Therefore, well placement and inter-well spacing optimizations is of greater importance in ultradeep, high pressure oil reservoirs to ensure higher ultimate oil recovery at lower costs. Furthermore, due to high cost of development of these reservoirs, the EOR strategy and commencement time for the selected EOR strategy are very critical.
This paper demonstrates how optimization of well placement, inter-well spacing, and startup time for miscible gas flooding can enhance the incremental and ultimate oil recoveries in an ultradeep, high pressure oil reservoir. To do this, a synthetic grid model was made to run different simulation scenarios on it. The model was initialized with rock and fluid properties within the range of those in the ultradeep, high pressure Wilcox formation in the Gulf of Mexico to ensure that it mimics an ultradeep, high pressure oil reservoir.
The results shows that the proposed optimization process for the selected EOR strategy is very beneficial and can improve the incremental recovery in an ultradeep, high pressure oil reservoir.
Similar optimization approaches to the one proposed in this paper can be used while studying other EOR strategies for an ultradeep, high pressure reservoir to acquire maximum recovery at a lower cost.